Precambrian Research 167 (2008) 316–338

Contents lists available at ScienceDirect

Precambrian Research

journal homepage: www.elsevier.com/locate/precamres

Superimposed Neoarchaean and Paleoproterozoic tectonics in the Terre Adélie Craton (East Antarctica): Evidence from Th–U–Pb ages on monazite and $^{40}Ar/^{39}Ar$ ages

Guillaume Duclaux[a,b,c,*], Yann Rolland[d], Gilles Ruffet[e], René-Pierre Ménot[a], Stéphane Guillot[f], Jean-Jacques Peucat[e], Mark Fanning[g], Patrice Rey[b], Arnaud Pêcher[f]

[a] Magmas et Volcans, CNRS, Université Jean Monnet, Saint Étienne, France
[b] Earth Byte Group, School of Geosciences, The University of Sydney, Sydney, NSW, Australia
[c] CSIRO Exploration and Mining, ARRC, Kensington, WA, Australia
[d] Géosciences Azur, CNRS, Université de Nice Sophia Antipolis, IRD, Nice, France
[e] Geosciences Rennes, CNRS, Université de Rennes 1, Rennes, France
[f] Laboratoire de Géodynamique des Chaînes Alpines, CNRS, Université Joseph Fourier, Grenoble, France
[g] Research School of Earth Sciences, Australian National University, Canberra, ACT, Australia

ARTICLE INFO

Article history:
Received 15 August 2007
Received in revised form
19 September 2008
Accepted 23 September 2008

Keywords:
Th–U–Pb dating of monazite
$^{40}Ar/^{39}Ar$ geochronology
Polyphase tectonic evolution
Craton reactivation
Strain localization

ABSTRACT

In order to understand the tectonic behaviour of a stabilized Neoarchaean continental crust during subsequent tectonic activity, we investigated the composite metamorphic basement along the Terre Adélie and George Vth Land coastline, also known as the Terre Adélie Craton (East Antarctica). Two domains are recognized: (1) a Neoarchaean basement, composed of granulite rocks to the east and overlain to the west by amphibolites, and (2) two Paleoproterozoic detrital basins overly the Neoarchaean crust and extend further west. New geochronological data from the Terre Adélie Craton define a tectonic evolution with three major peaks' activity. Th–U–Pb electron probe analyses of monazite from the Neoarchaean granulites constrain the main structuration event at *ca.* 2.45 Ga in agreement with zircon ages from throughout the Neoarchaean domain. Local resetting together with low temperature recrystallization of monazites occurred at *ca.* 1.7 Ga along hydrated anastomozing metre-scale shear zones. New $^{40}Ar/^{39}Ar$ ages obtained by stepwise heating techniques on amphibole, biotite and muscovite from both the Neoarchaean basement and the Paleoproterozoic basins, illustrate the differential evolutions of basement and its sedimentary cover during the major 1.7 Ga transpressive event. A final event at *ca.* 1.55–1.50 Ga is only recognized close to the Mertz Shear Zone (145°E) bounding the Terre Adélie Craton to the East. The new data allow us to propose detailed geological pictures of the Terre Adélie Craton geodynamic evolution, from the Neoarchaean to the Mesoproterozoic.

1. Introduction

Throughout Earth history and its related secular cooling, the deformation style of continental crust evolved in response to the crustal thermal regime and its stress state (Rey and Houseman, 2006). In recent orogens, cool and strong plates accommodate convergence through a combination of crustal underthrusting along narrow mountain belts and lateral escape of continental blocks along lithospheric strike-slip faults (Tapponnier et al., 1982). In contrast, Archaean continental lithospheres were warmer and accommodated convergence through homogeneous thickening and lateral ductile flow (Rey and Houseman, 2006; Cruden et al., 2006; Cagnard et al., 2006). Subsequently, unloading of warm orogenic domains during the decrease of the converging tectonic force favored orogen-parallel constrictional flow of the crust and tangential motions (Duclaux et al., 2007). The transition from Archaean to modern style geodynamics would appear to take place at around 2.0 Ga (Hamilton, 1998), coincident with the first occurrence of high pressure-low temperature subduction-related eclogites (Collins et al., 2004). Composite Archaean and Paleoproterozoic cratons, which underwent minor subsequent tectonic reactivation, are ideal terrains to study this major geodynamic evolution.

The Terre Adélie Craton (TAC) (Fig. 1) is composed of two crustal domains (Monnier et al., 1996): (1) a Neoarchaean to Siderian

* Corresponding author at: CSIRO Exploration and Mining, Australian Resources Research Centre , PO Box 1130, Bentley, WA 6102, Australia. Fax: +61 8 6436 8555.
E-mail address: guillaume.duclaux@csiro.au (G. Duclaux).

0301-9268/$ – see front matter.
doi:10.1016/j.precamres.2008.09.009

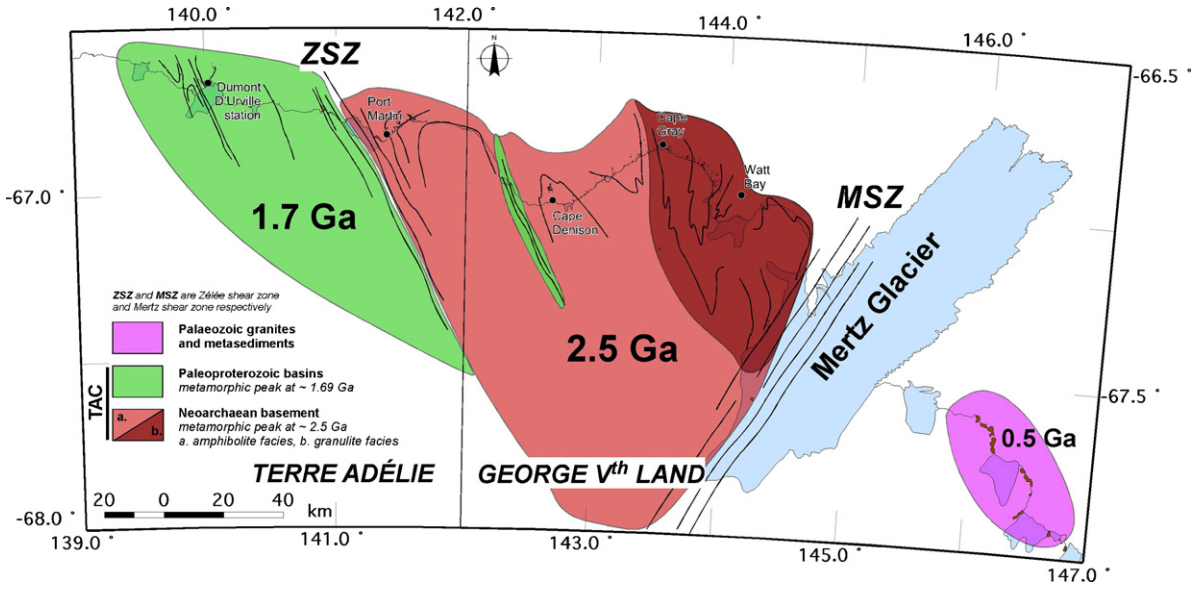

Fig. 1. Synthetic geological map of the Terre Adélie Craton (after Ménot et al., 2007). Green areas are Paleoproterozoic in age and correspond to the Dumont D'Urville (DDU) and Cape Hunter (CH) Basins; reddish areas are Archaean in age, the darker part to the east refers to the deep granulitic crust, and the brighter part refers to the intermediate to upper amphibolitic crust. MSZ denotes the Mertz shear zone and ZSZ denotes the Zélée shear zone. (For interpretation of the references to colour in this figure legend, the reader is referred to the web version of the article.)

(2.7–2.42 Ga) domain to the east, referred to below as the Neoarchaean domain, and (2) a Statherian (1.7 Ga) domain to the west, the Paleoproterozoic domain. These domains have been interpreted as two accreted terranes separated by a major tectonic boundary, the Zélée shear zone (Monnier et al., 1996; Pelletier et al., 1999). The main tectono-metamorphic event imprint in the Paleoproterozoic domain and resulting in the craton stabilization has been dated at about 1.7 Ga (Peucat et al., 1999a; Pelletier et al., 2002). In contrast, the Neoarchaean basement, which formed at *ca.* 2.8–2.7 Ga (Nd model ages and inherited zircons), underwent a polyphase evolution with a late and major event at *ca.* 2.5–2.4 Ga (Ménot et al., 1999, 2005; Peucat et al., 1999b). In this domain, ages at *ca.* 1.7 Ga are considered to be either local thermal resetting related to discrete shear zones (Oliver and Fanning, 2002; SHRIMP U–Pb zircon) or a regional pervasive thermal event (Di Vincenzo et al., 2007; $^{40}Ar/^{39}Ar$ laserprobe biotite). Consequently, the late tectonic and metamorphic history of the Neoarchaean domain is complex and controversial, and it appears necessary for the *P*, *T*, *t* evolution of this domain to differentiate between the two scenarios. Thus, the Paleoproterozoic evolution needs to be re-appraised in order to estimate the spatial extent of tectonic reworking in an already cooled Neoarchaean continental crust.

In this paper we address the following questions: (1) in terms of geochronological and structural overprinting within the Neoarchaean basement, is the 1.7 Ga resetting localized, or pervasive at a regional scale? (2) Which geodynamic context at 1.7 Ga can explain the relationships between the Neoarchaean and Paleoproterozoic domains? We propose a reassessment of the geodynamic evolution in the light of new geochronological data, via multimethod approach, combining Th–U–Pb dating of monazite and $^{40}Ar/^{39}Ar$ dating of amphibole, biotite and muscovite.

2. Geological setting

The Antarctic continent can be divided into two regions: West and East Antarctica, separated by the Transantarctic Mountains. While West Antarctica remains active today, East Antarctica is a stable craton, amalgamated during the Ross orogeny at *ca.* 530 Ma (Tingey, 1991; Fitzsimons, 2000, 2003). Most of the East Antarctic shield recorded tectono-thermal activity during the Grenvillian orogeny at *ca.* 1 Ga (Fitzsimons, 2000) with the noticeable exception of the Mawson continent (Fanning et al., 1995), which is considered to be devoid of any significant reworking after 1.5 Ga. The Mawson continent probably constitutes to a large portion of the unexposed East Antarctica basement, but its exact extent is rather difficult to constrain (see Fitzsimons, 2003). According to Fanning et al. (1995, 2003), it includes Terre Adélie and George Vth Land (the *Terre Adélie Craton* of Peucat et al., 1999a) and the Miller Range in the Central Transantarctic Mountains. Further north, it includes the South Australian's Gawler Craton and Curnamona Province. Within the Mawson continent, the composite Terre Adélie Craton (TAC) extends along the Antarctic coast between at least 136.4°E and 144.5°E and represents the easternmost area of the East Antarctic Shield (Fig. 1). The eastern boundary is marked by the prominent Mertz Shear Zone (144.3°E; Talarico and Kleinschmidt, 2003), which separates the Archaean and Proterozoic basement of the TAC from the Ross-Delamerian crystalline basement including granitoids and metasediments from the Cape Webb area (Fanning et al., 2002, 2003; Di Vincenzo et al., 2007). The Ross-Delamerian rocks mark the western boundary of the Ross orogen that extends eastwards into Oates Land. The western boundary is not properly defined due to the lack of exposure and suitable geophysical information. Rocher X (136.4°E) is the westernmost outcrop related to the TAC. Further west, outcrops in the Windmill Islands display Archaean and Proterozoic material strongly overprinted by late Mesoproterozoic events (between 1340 Ma and 1130 Ma, Fitzsimons, 2003).

The TAC exposure is restricted to hectometre to kilometre square islands and capes scattered along the coastline and to a few nunataks, mainly in the inland area of Commonwealth Bay (Fig. 2). Extremely well-exposed polished glacial surfaces and the absence of any alteration allow for excellent field analysis in the scattered islands along the coast. Within the basement

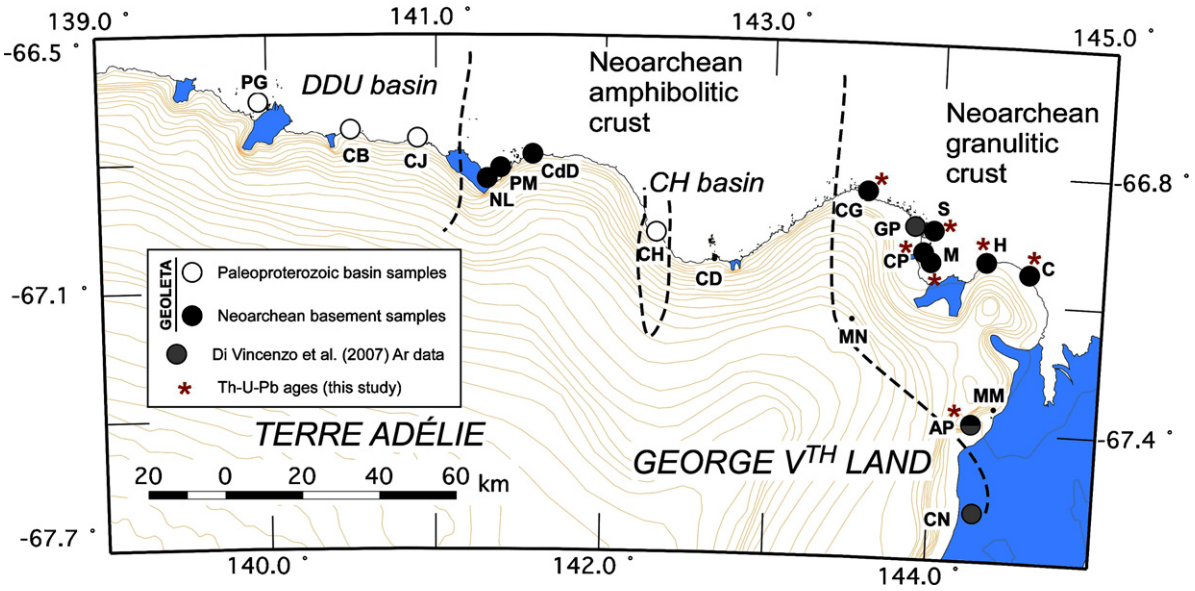

Fig. 2. Detailed samples location. Filled circles indicate the location of new ages obtained for the Neoarchaean domain, and open circles indicate those of the Paleoproterozoic domain. Grey circles indicate the location of samples dated by Di Vincenzo et al. (2007). From West to East, PG: Pointe Géologie, CB: Cap Bienvenüe, CJ: Cap Jules, NL: Nunatak Lacroix, PM: Port Martin, CdD: Cap de la Découverte, CH: Cape Hunter, CD: Cape Denison, MN: Madigan Nunatak, CG: Cape Grey, GP: Garnet Point, S: Stillwell Island, CP: Cape Pigeon, M: Moyes Archipelago, H: Hodgemann Archipelago, C: Close Island, MM: Murchinson Mounts, AP: Aurora Peak, CN: Correll Nunatak.

of the TAC, two domains are recognized differentiated by their ages and lithologies (Monnier et al., 1996; Ménot et al., 1999; Peucat et al., 1999a). (1) To the East, a complex Neoarchaean crust (2.8–2.42 Ga) crops out from the Mertz glacier (144.3°E) to the Zélée glacier (141.31°E). (2) Overlaying and to the west of this domain are two Paleoproterozoic metasedimentary domain known as the Cape Hunter basin the Dumont D'Urville basin (DDU) respectively. The latter probably extends further west to Rocher Janet (139.1°E), Rocher X and Rocher Mathieu (136.4°E) (Ménot et al., 2007).

2.1. The Neoarchaean domain

The Neoarchaean crust can be subdivided into two metamorphic units (Ménot et al., 2005): (1) a granulite facies unit to the east, and (2) an amphibolite facies unit to the west.

(1) The deep crust is composed of both orthogneisses of felsic to mafic composition and metasediments, mainly metapelites and subordinate marbles and quartzites. This lower crust underwent a polyphase and long-lived tectonic and metamorphic evolution from granulite facies conditions (peak conditions of $T \geq 800$ °C and P up to 9 ± 1.5 kbar), down to amphibolite facies conditions (550 °C, 5 kbar) for subsequent retrogression (Pelletier et al., 2001). This evolution occurred between ~2.5 Ga (initial granulitic event) and 2.42 Ga (retrogression and related partial melting; Ménot et al., 2005 and references therein). At a regional scale, two successive metamorphic foliations are identified, observed in the granulite and amphibolite facies paragneneses respectively. The granulite foliation, when preserved from transposition, is relatively flat, gently dipping to the south. The amphibolite foliation is steeper and associated with centimetre to hectometre-scale isoclinal folds and partial melting (Ménot et al., 2005). Horizontal boudinaged mafic rods and calc-silicate layers, parallel to the N140 mineral stretching lineation, indicate horizontal flow in the deep crust (Duclaux et al., 2007). These later fabrics are compatible with the dome shape structure of the deep crustal part of the Neoarchaean domain.

(2) In the intermediate to upper crust, gneissic basement is intruded by prominent monzogranodiorite plutons and laccoliths together with aluminous pink granites and mafic dikes. All granitoids display complex mingling and assimilation features (Duclaux, 2007). The syntectonic intrusion of the monzogranodiorites and the coeval amphibolite facies metamorphism was dated at *ca.* 2.44 Ga by U–Pb zircons in the Port Martin area (Monnier et al., 1996; Peucat et al., 1999b). The regional foliation trend changes from N70 to N150 approaching the Zélée shear zone to the west and the narrow Cape Hunter basin to the east (Fig. 1).

Localized centimetre to metre-scale steep shear zones are present in both crustal levels. These shear zones display a conjugate dextral and sinistral sense of shear, with a dominant dextral motion toward the East. They contain hydrated greenschist facies biotite–chlorite assemblages and act as a plumbing system for fluid circulation (Duclaux, 2007).

2.2. The Paleoproterozoic domain

This domain is composed of two distinct Paleoproterozoic basins (Figs. 1 and 2):

(1) To the east (142.1°E), the narrow basin of Cape Hunter (CH) between the Cape Denison and the Point Alden is characterized by the exposure of a 500-m wide zone of phyllites pinched within the intermediate Neoarchaean crust. The contacts between the Neoarchaean basement and the basin have not been identified in the field due to ice cover. The Cape Hunter sediments are mainly pelitic with a slight volcanic component dated by a SHRIMP zircon age at 1765 ± 8 Ma (Oliver and Fanning, 1997). Subsequent recrystallization occurred under greenschist facies conditions (350–500 °C at 4–5 kbar) (Oliver and Fanning, 1997). These phyllites contain a penetrative vertical foliation associated with upright folds and associated vertical axial planes (Ménot et al., 2005).

Table 1
Samples localization and description.

Sample	Domain	Location place name	Latitude	Longitude	Lithology	Mineralogy	Fabric
RPM98-119	Neoarchean granulitic crust	Aurora Peak	67°23.20′S	144°14.24′E	Noritic gneiss	opx pl qtz	Mylonite
RPM98-124b	–	Aurora Peak	67°23.20′S	144°14.24′E	Noritic gneiss	opx pl qtz	Ultra-mylonite
GD04-174	–	Close Island	67°01.56′S	144°33.40′E	Migmatite	bt qtz pl gt sil	Migmatitic foliation with preserved palaeosome
GD04-160a	–	Hodgeman Island	66°59.78′S	144°16.29′E	Migmatite	opx gt bt crd sp co pl qtz ilm	Partial melting textures with retrogression coronnas
GD04-162	–	Hodgeman Island	66°59.78′S	144°16.32′E	Granulitic migmatite	opx gt bt crd sp co pl qtz ilm	Partial melting textures with retrogression coronas
RPM03-37	–	Moyes Island	67°00.27′S	143°55.51′E	Aluminous gneiss	gr sill bt st qt pl oxy tour	Partial melting textures
GD04-155	–	Moyes Island	67°00.27′S	143°55.51′E	Paragneiss	qt pl bt gr	Foiated with lepidoblastic texture
GD04-147	–	C Island	66°56.86′S	143°53.99′E	Orthogneiss	pl qtz bt chl	Mylonite with c/s texture
GD04-148	–	C Island	66°56.85′S	143°53.98′E	Restitic mafic granulite	opx pl bt gr qtz sp ilm	Isogranular texture with gr coronas
Gd04-149	–	C Island	66°56.84′S	143°53.97′E	Tonalite	bt pl qtz pert ilm gt	Isotropic
GD04-130	–	Cape Pigeon	66°58.68′S	143°53.72′E	Orthogneiss	bt chl micr pl qtz	Boudinage and foliation
GD04-133	–	Cape Pigeon	66°58.66′S	143°53.67′E	Orthogneiss	opx bt gr pl micr	Recrystallized
GD04-124	–	Stillwell Island	66°58.65′S	143°53.61′E	Granite	qts peth gr bt	Isotropic
GD04-183	–	Cape Gray - East	66°50.71′S	143°32.62′E	Amphibolite	gr ep cc amp oxy bt	Fluid induced recrystallization
GD04-190	–	Cape Gray - East	66°50.72′S	143°32.68′E	Paragneiss	qtz pl bt gr	Foliation underlined by bt
AP98-24	Paleoproterozoic basin	Cape Hunter	66°57.02′S	142°20.19′E	Phylite	qtz msc chl gr	Pervasive schistosity
GD04-216	Neoarchean amphibolitic crust	Cap de la Découverte	66°46.55′S	141°33.54′E	Ultramafic xenolith	amp bt pl opx cpx	Isogranular
PMA13	–	Port Martin	66°48.85′S	141°23.98′E	Layered gneiss xenolith	amp bt sph pl qtz	Modal layering
PMA14A	–	Port Martin	66°48.86′S	141°23.98′E	Mylonitic mafic gneiss	cpx amp bt ser	Strongly foliated, boudinage
PMA14C	–	Port Martin	66°48.87′S	141°23.98′E	Syn-kinematic mafic dyke	amp bt pl ser epd	Foliated
JJP98-6A	Paleoproterozoic basin	Cap Jules	66°44.82′ S	140°55.03′ E	Meta-gabbro	amp bt pl opx qtz	Undeformed
JJP98-17	–	Cap Jules	66°44.82′ S	140°55.03′ E	Amphibolite	cpx amp pl	Undeformed but recrystallized
AP99-36A	–	Cap Bienvenüe	66°43.20′ S	140°30.23′ E	Mafic gneiss	opx amp bt qtz pl	Foliated
JJP98-4B	–	Cap Bienvenüe	66°43.20′ S	140°30.23′ E	Mafic gneiss	opx amp bt qtz pl micr	Foliated
OM110-1	–	Pointe Géologie	66°39.70′ S	139°59.03′ E	Anatectic gneiss	qtz bt kfs pl gr	Isotropic with restitic textures
DDU89	–	Pointe Géologie	66°41.23′ S	139°54.13′ E	Anatectic melanosome	qtz perth gr bt	Isotropic

Table 2
Monazites ages, chemical and textural characteristics.

Analyse	Location	*n*	Associated fabric	ThO_2	UO_2	PbO	Age (Ma)	2σ error (Ma)	ThO_2*	UO_2*	PbO/ThO_2*
	Aurora Peak										
		8	*mnz in foliation*	*1.67–8.83*	*0.05–0.29*	*0.13–0.67*	***1619***	***±48***	***MSWD = 0.97***		
		4	*mnz in foliation*	*2.52–17.80*	*0.15–0.21*	*0.27–1.48*	***1995***	***±52***	***MSWD > 5***		
Detailed analyses											
RPM98-124B	*Aurora Peak*										
1				8.8301	0.1217	0.6680	1646.80	±44.63	9.2762	2.5310	0.0720
2				17.8033	0.1548	1.4752	1826.71	±32.27	18.3819	4.9186	0.0803
3				6.9581	0.0543	0.5340	1703.11	±54.32	7.1583	1.9414	0.0746
4				1.6671	0.0731	0.1255	1493.45	±148.32	1.9307	0.5352	0.0650
RPM98-119	*Aurora Peak*										
1				3.8344	0.1334	0.3078	1630.02	±76.37	4.3225	1.1816	0.0712
2				4.0629	0.2895	0.3454	1550.67	±65.38	5.1131	1.4094	0.0676
3				3.6025	0.1281	0.2873	1616.29	±80.64	4.0703	1.1142	0.0706
4				6.0942	0.2105	0.5932	1954.12	±57.91	6.8924	1.8180	0.0861
5				2.5899	0.2560	0.2504	1627.88	±81.63	3.5260	0.9643	0.0710
6				2.3438	0.0784	0.1769	1544.11	±114.97	2.6281	0.7248	0.0673
7				2.6128	0.1846	0.3255	2204.51	±99.72	3.3342	0.8534	0.0976
8				2.5162	0.1575	0.2740	1995.77	±103.15	3.1161	0.8181	0.0879
	Fletcher C										
		6	*mnz in foliation with biotite*	*1.90–4.55*	*0.15–0.22*	*0.21–0.38*	***1712***	***±34***	***MSWD = 2.81***		
		10	*mnz in foliation*	*1.99–4.04*	*0.15–0.27*	*0.24–0.41*	***1897***	***±28***	***MSWD = 1.59***		
Detailed analyses											
GD04-190	*Fletcher C*										
1				3.3880	0.1495	0.2980	1727.22	±41.50	3.9406	1.0662	0.0756
2				3.1790	0.1565	0.2850	1732.41	±42.88	3.7576	1.0161	0.0758
3				2.0030	0.2720	0.2450	1849.29	±47.76	3.0216	0.8069	0.0811
4				2.1240	0.2468	0.2530	1888.05	±48.60	3.0525	0.8115	0.0829
5				2.0460	0.2172	0.2510	1985.40	±52.72	2.8724	0.7551	0.0874
6				1.8970	0.2219	0.2120	1779.25	±51.12	2.7216	0.7324	0.0779
7				1.9940	0.2659	0.2420	1846.54	±47.76	2.9893	0.7985	0.0810
8				1.9780	0.1814	0.2080	1789.63	±53.48	2.6530	0.7131	0.0784
9				3.9010	0.1879	0.4080	2004.47	±41.12	4.6173	1.2109	0.0884
10				4.0350	0.1503	0.3900	1925.43	±40.82	4.6028	1.2181	0.0847
11				3.2360	0.2129	0.3330	1878.28	±42.19	4.0362	1.0741	0.0825
12				3.3560	0.2197	0.3190	1747.36	±39.37	4.1698	1.1258	0.0765
13				3.5480	0.2417	0.3620	1851.73	±38.99	4.4535	1.1887	0.0813
14				3.8790	0.1890	0.3770	1870.19	±39.29	4.5885	1.2221	0.0822
15				4.5500	0.2216	0.3780	1615.68	±31.97	5.3593	1.4673	0.0705
16				3.8620	0.1993	0.3820	1884.84	±39.06	4.6117	1.2262	0.0828
	Cape Pigeon										
		12	*mnz in foliation*	*1.63–6.78*	*0.07–0.15*	*0.14–0.52*	*1697*	***±44***	***MSWD = 0.37***		
		4	*mnz in feldpar*	*3.17–6.20*	*0.10–0.16*	*0.30–0.57*	*1869*	***±70***	***MSWD = 1.20***		
Detailed analyses											
GD04-130	*Cape Pigeon*										
1				4.0042	0.1229	0.3572	1822.89	±77.90	4.4632	1.1949	0.0800
2				3.4761	0.0954	0.2910	1734.70	±86.52	3.8291	1.0351	0.0760
3				3.1666	0.0969	0.3018	1939.77	±95.06	3.5335	0.9336	0.0854
4				3.8075	0.0927	0.3189	1752.70	±82.17	4.1511	1.1199	0.0768
5				4.0839	0.0981	0.3418	1753.31	±77.67	4.4476	1.1998	0.0769
6				1.6330	0.0653	0.1422	1732.41	±151.29	1.8744	0.5069	0.0759
7				6.5167	0.1465	0.5332	1724.62	±54.17	7.0581	1.9100	0.0755
8				6.7836	0.1267	0.5206	1642.99	±53.48	7.2479	1.9784	0.0718
9				5.6803	0.1226	0.4632	1724.01	±60.73	6.1334	1.6599	0.0755
10				6.1966	0.1250	0.5693	1938.10	±59.89	6.6695	1.7623	0.0854
11				5.8124	0.1620	0.5066	1799.39	±59.43	6.4161	1.7222	0.0790
12				4.0882	0.1085	0.3268	1665.57	±75.76	4.4866	1.2218	0.0728
GD04-133	*Cape Pigeon*										
1				4.0293	0.1808	0.3353	1636.28	±78.43	4.6911	1.2816	0.0715
2				2.9687	0.1553	0.2615	1688.92	±98.88	3.5405	0.9619	0.0739
3				2.8583	0.1290	0.2387	1640.40	±103.84	3.3309	0.9096	0.0717
4				3.3470	0.1244	0.2303	1398.54	±89.80	3.7915	1.0610	0.0607
	Stilwell Island										
		6	*in quartz + feldspar foliation*	*3.26–11.95*	*0.07–0.31*	*0.41–1.44*	***2468***	***±44***	***MSWD = 0.70***		
		9	*mnz in garnet*	*3.49–12.71*	*0.08–0.23*	*0.48–1.52*	***2586***	***±38***	***MSWD = 0.47***		
		1	*mnz in garnet*				*3386*	*±84*			*relictual ?*
Detailed analyses											
GD04-124	*Stilwell Island*										
1				11.9451	0.2099	1.4385	2514.72	±46.39	12.8004	3.1418	0.1124
2				10.2258	0.1919	1.2695	2575.30	±50.89	11.0143	2.6800	0.1153

Table 2 (*Continued*)

Analyse	Location	*n*	Associated fabric	ThO_2	UO_2	PbO	Age (Ma)	2σ error (Ma)	ThO_2*	UO_2*	PbO/ThO_2*
3				10.7233	0.1850	1.3452	2613.75	±50.20	11.4878	2.7795	0.1171
4				10.1032	0.1726	1.1618	2414.02	±49.36	10.7967	2.6873	0.1076
5				10.6252	0.1555	1.2869	2554.09	±50.20	11.2624	2.7487	0.1143
6				10.8524	0.1722	1.3491	2604.75	±50.05	11.5632	2.8014	0.1167
7				8.2189	0.3055	1.0211	2425.16	±51.80	9.4481	2.3485	0.1081
8				3.4856	0.1420	0.4777	2619.40	±92.77	4.0727	0.9848	0.1173
9				3.5892	0.1115	0.4799	2642.75	±94.99	4.0520	0.9763	0.1184
10				3.2622	0.1168	0.4115	2469.56	±97.50	3.7349	0.9227	0.1102
11				4.5789	0.1233	0.7847	3336.87	±84.46	5.1553	1.1030	0.1522
12				9.1125	0.0814	1.0434	2474.59	±55.24	9.4423	2.3305	0.1105
13				9.3972	0.0747	1.0890	2511.37	±55.08	9.7013	2.3820	0.1123
14				8.4356	0.0791	1.0000	2551.50	±58.67	8.7598	2.1386	0.1142
15				8.9397	0.2331	1.1739	2643.51	±53.71	9.9074	2.3868	0.1185
16				12.7102	0.1627	1.5205	2541.73	±46.16	13.3755	3.2702	0.1137
	Watt Bay										
		4	*mnz in foliation*	*1.23–2.65*	*0.12–0.38*	*0.13–0.28*	***1755***	***±54***	***MSWD = 2.37***		
		2	*mnz in foliation*	*1.41–1.44*	*0.19–1.28*	*0.19–0.23*	***2094***	***±180***	***MSWD = 0.09***		*relictual ?*
Detailed analyses											
GD04-155	*Watt Bay*										
1				1.2328	0.1231	0.1277	1729.81	±166.78	1.6879	0.4567	0.0757
2				2.1331	0.3332	0.2579	1751.63	±88.04	3.3673	0.9090	0.0766
3				1.4077	0.1910	0.1946	2062.15	±138.70	2.1408	0.5578	0.0909
4				1.4378	0.2767	0.2340	2116.32	±118.10	2.5066	0.6489	0.0934
RPM03-37	*Watt Bay*										
1				2.6470	0.2625	0.2640	1673.81	±42.11	3.6114	0.9829	0.0731
2				2.0730	0.3789	0.2790	1826.40	±38.83	3.4882	0.9340	0.0800
	Hodgeman Arch.										
		8	*mnz in garnet and feldspar*	*2.84–5.80*	*0.10–0.30*	*0.31–0.71*	***2282***	***±40***	***MSWD = 0.70***		
		14	*mnz in garnet and feldspar*	*3.12–16.93*	*0.07–0.44*	*0.34–1.99*	***2477***	***±22***	***MSWD = 2.66***		
Detailed analyses											
GD04-162	*Hodgeman Arch.*										
1				7.0360	0.2548	0.8670	2414.47	±35.93	8.0597	2.0063	0.1076
2				6.7390	0.1559	0.8170	2482.53	±39.52	7.3714	1.8176	0.1108
3				7.2470	0.2870	0.9180	2449.42	±35.48	8.4056	2.0824	0.1092
4				16.9310	0.2798	1.9890	2466.81	±27.85	18.0633	4.4634	0.1101
5				5.4960	0.2944	0.7100	2390.06	±37.77	6.6746	1.6672	0.1064
6				8.4810	0.2465	1.0350	2448.96	±34.26	9.4760	2.3475	0.1092
7				5.3190	0.2971	0.6540	2271.19	±36.77	6.4899	1.6468	0.1008
8				8.0780	0.4355	1.1350	2572.86	±33.11	9.8667	2.4024	0.1150
9				7.5230	0.3757	0.9310	2324.30	±32.12	9.0139	2.2713	0.1033
10				7.5590	0.4291	1.0740	2576.52	±33.72	9.3224	2.2687	0.1152
GD04-160A	*Hodgeman Arch.*										
1				2.8448	0.0508	0.3088	2282.33	±113.75	3.0453	0.7714	0.1014
2				4.0971	0.0781	0.4507	2301.41	±86.14	4.4060	1.1133	0.1023
3				4.0478	0.0732	0.4684	2419.66	±88.73	4.3423	1.0800	0.1079
4				3.2890	0.0724	0.3364	2129.75	±97.96	3.5693	0.9218	0.0942
5				3.1181	0.0835	0.3765	2443.62	±104.06	3.4549	0.8565	0.1090
6				4.3900	0.0799	0.5288	2509.84	±84.76	4.7153	1.1581	0.1121
7				5.1275	0.1036	0.5514	2244.80	±73.01	5.5346	1.4088	0.0996
8				5.1962	0.1494	0.6187	2396.93	±71.33	5.7949	1.4459	0.1068
9				5.7969	0.0964	0.6158	2246.32	±67.52	6.1757	1.5717	0.0997
10				5.6919	0.1506	0.7563	2668.38	±70.88	6.3193	1.5167	0.1197
11				5.8448	0.1391	0.6963	2437.67	±67.52	6.4056	1.5893	0.1087
12				6.0775	0.2165	0.7488	2418.75	±62.94	6.9477	1.7285	0.1078
	C Island										
		6	*mnz in foliation*	*3.37–13.27*	*0.18–0.35*	*0.21–1.08*	***1696***	***±44***	***MSWD = 0.76***		
		14	*mnz in garnet and feldspar*	*1.84–8.82*	*0.15–0.50*	*0.45–1.14*	***2629***	***±22***	***MSWD = 2.50***		
		11	*mnz in garnet and feldspar*	*5.41–8.84*	*0.14–0.49*	*0.70–1.02*	***2433***	***±34***	***MSWD = 1.18***		
Detailed analyses											
GD04-147	*C Island*										
1				8.3729	0.2210	0.6663	1659.16	±48.83	9.1838	2.5027	0.0726
2				3.5182	0.1783	0.3109	1702.04	±86.06	4.1752	1.1328	0.0745
3				3.3708	0.1882	0.3112	1747.06	±89.26	4.0678	1.0983	0.0765
4				3.7710	0.2161	0.3161	1589.89	±79.42	4.5583	1.2514	0.0693
5				13.2664	0.3457	1.0805	1697.77	±36.93	14.5400	3.9461	0.0743
6				10.5642	0.2807	0.8854	1741.41	±43.18	11.6035	3.1344	0.0763

Table 2 (*Continued*)

Analyse	Location	*n*	Associated fabric	ThO_2	UO_2	PbO	Age (Ma)	2σ error (Ma)	ThO_2*	UO_2*	PbO/ThO_2*
Detailed analyses											
GD04-148	*C Island*										
1				6.3650	0.2047	0.8620	2663.80	±41.20	7.2172	1.7336	0.1194
2				6.8540	0.1514	0.7810	2353.44	±37.46	7.4573	1.8715	0.1047
3				6.7090	0.1849	0.9090	2705.76	±41.50	7.4837	1.7861	0.1215
4				6.6090	0.1595	0.8470	2602.77	±41.05	7.2671	1.7613	0.1166
5				4.2840	0.3421	0.6790	2657.09	±42.34	5.7062	1.3725	0.1190
6				7.0770	0.2104	0.9110	2565.08	±38.15	7.9402	1.9351	0.1147
7				6.7050	0.2004	0.8270	2466.20	±37.92	7.5157	1.8575	0.1100
8				2.3710	0.4531	0.5460	2825.09	±45.39	4.3030	1.0091	0.1269
9				8.0040	0.1915	1.0270	2607.50	±37.61	8.7949	2.1301	0.1168
10				3.2090	0.2151	0.4600	2521.90	±50.74	4.0859	1.0022	0.1126
11				8.7060	0.2055	1.1130	2601.70	±36.16	9.5537	2.3158	0.1165
12				8.8220	0.1917	1.1350	2633.59	±36.62	9.6165	2.3201	0.1180
13				6.8210	0.2144	0.8780	2550.74	±38.60	7.6988	1.8802	0.1140
14				1.8400	0.5004	0.4540	2605.82	±43.95	3.9030	0.9466	0.1163
Detailed analyses											
GD04-149	*C Island*										
1				8.2773	0.1549	0.9616	2423.32	±61.26	8.9005	2.2126	0.1080
2				5.9703	0.2890	0.8192	2561.11	±68.28	7.1552	1.7451	0.1145
3				8.6019	0.1364	1.0042	2458.27	±60.27	9.1534	2.2645	0.1097
4				6.3944	0.2235	0.8115	2489.70	±68.13	7.3018	1.7988	0.1111
5				5.4092	0.4937	0.8843	2648.39	±63.78	7.4589	1.7966	0.1186
6				5.4503	0.2431	0.7026	2450.33	±72.33	6.4315	1.5932	0.1092
7				7.4841	0.4676	0.9603	2315.60	±54.24	9.3375	2.3558	0.1028
8				7.9919	0.1813	0.9179	2365.95	±60.50	8.7154	2.1835	0.1053
9				8.4724	0.1779	1.0077	2457.05	±59.74	9.1914	2.2743	0.1096
10				8.8380	0.1654	1.0164	2400.74	±58.21	9.5013	2.3692	0.1070
11				6.5900	0.2143	0.8617	2577.90	±68.28	7.4711	1.8174	0.1153

(2) To the west of the Neoarchaean domain, the Dumont D'Urville basin (DDU) is exposed in the Cap Jules (140.5°E), the Cap Bienvenüe (140.3°E), and the Pointe Géologie Archipelago (139.8–140°E). The metasedimentary sequence in these three areas are dominated by metapelites including subordinate metagraywackes and dismembered layers of metafelsites and calc-silicates (Monnier et al., 1996). These lithologies are affected by extensive partial melting and intruded by synkinematic granitic and mafic dykes, and locally by synkinematic gabbroic plutons (Pelletier et al., 2002). Metapelites are equilibrated under HT–LP metamorphic conditions, with peak conditions of 650–750 °C and 4–6 kbar (Monnier, 1995; Pelletier et al., 2002). The evolution of the DDU basin is bracketed by the 1.72 Ga minimum sediment deposition age, and the 1.69 Ga peak of metamorphism (Peucat et al., 1999a). Regional foliation trajectories reveal two main structure types, both associated with migmatization: (1) large dome-shaped structures with a composite foliation that ranges from flat-lying to gently dipping, and (2) kilometre-scale vertical shear zones (Pelletier et al., 2002; Gapais et al., 2008). These authors proposed that the relative volume of the vertical shear zones widened at the expense of the domes. This coincides with an increasing dextral strike slip component when approaching the Neoarchaean domain, which acted as a rigid block (Fig. 1 in Pelletier et al., 2002).

3. Analytical settings

3.1. Electron microprobe dating of monazite

Monazite from 13 samples (described in Table 1) have been dated with a Cameca Camebax and Cameca SX100 electron microprobes using the method described in Goncalves et al. (2004). The detailed analytical protocols are summarized in Appendix A. Analyses were undertaken using an accelerating voltage of 15 kV and beam current of 150 nA and a electron beam radius of around 3–4 μm. Ages have been calculated following the statistical Th–U–Pb method of Montel et al. (1996) and are summarized in Table 2. The *in situ* analyses have been modelled according to a least-squares fit equation for a Gaussian distribution (Montel et al., 1996). The Chi square test (Montel et al., 1996) and the Mean Squared Weighted Deviation (MSWD) (Wendt and Carl, 1991) are used as "goodness of fit tests" for validity of the model. The SEM (Fig. 3B) data was collected at the CSIRO X-Ray laboratory in Kensington (WA) using a Philips (FEI) XL40 controlled pressure SEM fitted with an EDAX energy dispersive X-ray spectrometer and a Robinson Back Scattered Electron (BSE) detector. The SEM was operated in controlled pressure mode with a chamber pressure between 0.1 mbar and 0.5 mbar and an accelerating voltage of 30 kV.

3.2. ^{39}Ar–^{40}Ar analytical procedure

Single grains of biotite (14 samples), muscovite (2 samples) and amphibole (3 samples) were handpicked under a binocular microscope from 125 μm to 250 μm mineral fractions, after using magnetic and heavy liquid separation methods. Samples were wrapped in aluminium foil to form small packets (11 mm × 11 mm) that were stacked up to form a pile within which standards were inserted every 11–12 samples. The irradiation standard was amphibole Hb3gr (1071.7 ± 5.4 Ma; Turner et al., 1971; Roddick, 1983; Jourdan et al., 2006). The irradiation was performed at the McMaster reactor (Hamilton, Canada) and lasted 120 h (5C position, total fluence of 9×10^{18} n cm^{-2}). The sample and standards arrangement within the irradiation allowed us to monitor the flux gradient with a precision of ±0.2%.

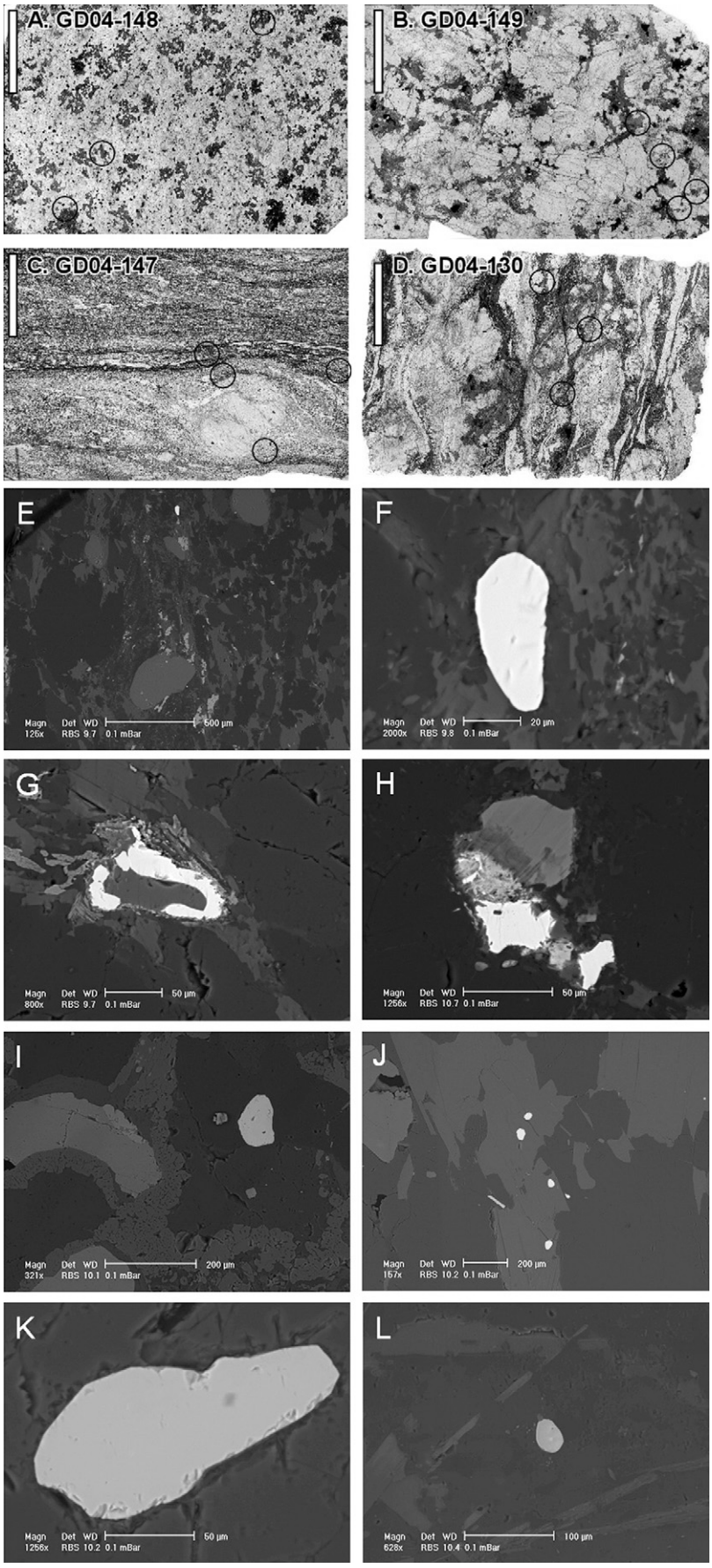
A. GD04-148
B. GD04-149
C. GD04-147
D. GD04-130
E
Magn Det WD 500 µm
126x RBS 9.7 0.1 mBar
F
Magn Det WD 20 µm
2000x RBS 9.8 0.1 mBar
G
Magn Det WD 50 µm
800x RBS 9.7 0.1 mBar
H
Magn Det WD 50 µm
1256x RBS 10.7 0.1 mBar
I
Magn Det WD 200 µm
321x RBS 10.1 0.1 mBar
J
Magn Det WD 200 µm
157x RBS 10.2 0.1 mBar
K
Magn Det WD 50 µm
1256x RBS 10.2 0.1 mBar
L
Magn Det WD 100 µm
628x RBS 10.4 0.1 mBar

The step-heating experiments conducted on single grains have been described by Ruffet et al. (1991, 1995) and Rolland et al. (2008). CO_2-laser step-heating experiments were analysed on Map215® and VG3600® mass spectrometers. Blanks were performed routinely every three steps, and subtracted from subsequent sample gas fractions. Isotopic measurements were corrected for K, Ca and Cl isotopic interferences and mass discrimination. It is commonly acknowledged that a plateau age is obtained when the apparent ages of at least three consecutive steps, comprising a minimum of 70% of the ^{39}Ar released, agree within 2σ error bars with the integrated age of the plateau segment. Nevertheless, pseudo-plateau ages can be calculated with less than 70% of the ^{39}Ar released, especially when they can be related to multiple mineral components within the dated crystal. All errors are quoted at the 1σ level and do not include the errors on the $^{40}Ar^*/^{39}Ar_K$ ratio and age of the monitor. The error on the $^{40}Ar^*/^{39}Ar_K$ ratio of the monitor is included in the plateau age calculation.

4. Results

The results obtained for Th–U–Pb electron probe dating are reported in Table 2 and summarized in Figs. 3 and 4. The $^{40}Ar/^{39}Ar$ results are displayed in Table 3 and shown in Figs. 5–7. Data are described according to their geological context and geographical location (Fig. 2).

4.1. The Neoarchaean domain

4.1.1. The eastern granulite Neoarchaean crust

Monazite ages from 13 samples from the granulite crust exposed from the west of the Mertz glacier to Cape Gray are detailed below (SEM pictures of representative samples presented in Fig. 3, analytical data presented in Table 2).

The 123 *in situ* analyses of monazites are presented as separated Gaussian curves with time in the abscissa (in Ma) and are compiled on a cumulative Gaussian curve corresponding to age frequencies (Fig. 4A). This curve displays two clear age peaks at 2502 ± 12 Ma and 1788 ± 14 Ma with MSWD greater than 5. The age of the two populations are not completely representative of the geological event as they include some inheritance and mixing ages due to Pb loss (see below for discussion). Nevertheless, these data clearly indicate two stages of monazite growth. In a PbO versus ThO_2^* diagram (Suzuki et al., 1991) (Fig. 4B), most of the data lie along two linear trends corresponding to a 2.45 Ga (filled circle analyses) and a 1.7 Ga (filled squared analyses) event ages. Anlayses scattered between these two pseudo-isochrons correspond to monazites from mylonitic samples with localized biotite–chlorite shear bands. With the exception of the two samples GD04-147 and RPM98-124B, all the monazites lying on the 1.7 Ga pseudo-isochron have ThO_2^* content lower than 7% (ThO_2 lower than 3%, see Table 2).

Detailed analytical results for each sample are given in Appendix B. Here, we develop results from three samples from C Island (in the Watt Bay) selected for their evident field relationships. They clearly illustrate the general evolution of the Neoarchaean granulite crust. Intra-foliation elongated monazites from a fluid-rich mylonitic shear zone (GD04-147: with qt + pl + bt + chl assemblage) (Fig. 3C and E–G) are dated at 1696 ± 44 Ma (MSWD 0.76, $n = 6$). This shear zone cross-cuts an isotropic hectometre tonalitic body (GD04-149, Fig. 3B and L) with rounded monazites included in plagioclase dated at 2433 ± 34 Ma (MSWD 1.18, $n = 11$) that includes foliated mafic xenoliths (GD04-148, Fig. 3A and I) with rounded monazites dated at 2629 ± 22 Ma (MSWD 2.50, $n = 14$). Both the tonalitic orthogneiss and its mafic xenoliths record granulite facies conditions (Duclaux, 2007). In contrast to monazites

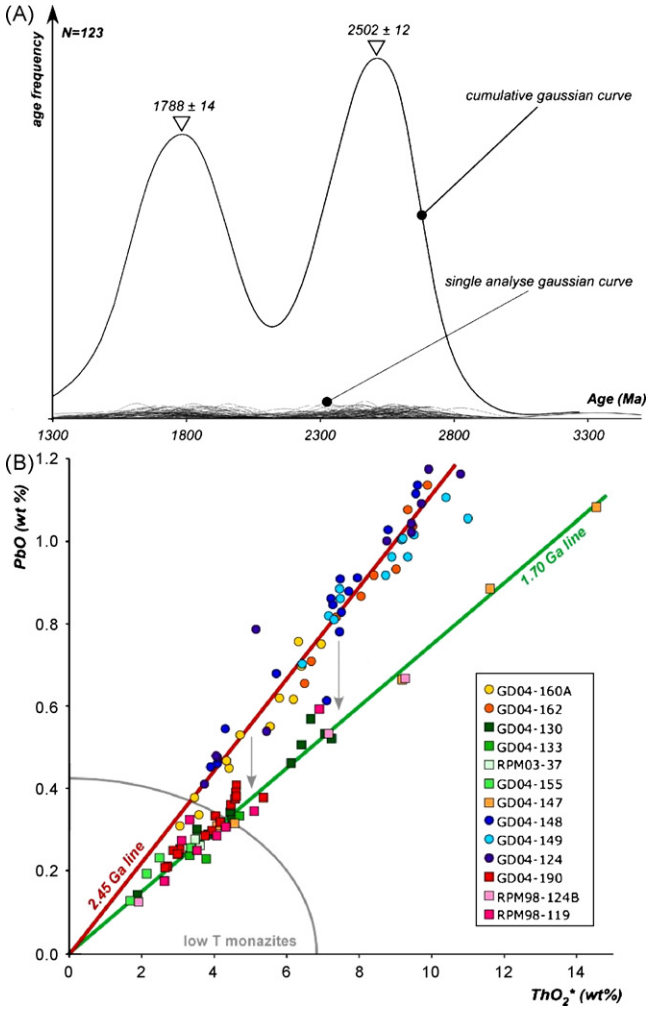

Fig. 4. Monazites data for the Deep Neoarchaean crust. (A) Frequency versus age diagram: age frequencies are represented by a Gaussian cumulative distribution curve and indicate two main monazites growth events. (B) PbO versus ThO_2^* diagram (after Suzuki et al., 1991): most analyses plot on two distinct trends relative to monazites growth age at 2.45 Ga and 1.70 Ga. Intermediate analyses are interpreted to reflect partial resetting of 2.45 Ga monazites or age mixing probably linked to later fluid circulation along narrow shear zones at about 1.7 Ga. (For interpretation of the references to colour in this figure legend, the reader is referred to the web version of the article.)

Fig. 3. Monazites locations for representative samples of the TAC. A–D: thin section photography of samples GD04-149, GD04-149, GD04-147 and GD04-130, indicating (circles) the position of monazites analysed for this study. A and B represent preserved samples from any 1.7 Ga tectonic reworking. C and D correspond to hydrated shear zones where deformation localized during the 1.7 Ga event. Scale is given by the vertical bar of 1 cm in every picture. (E–L) BSE pictures of monazites from mylonitic samples GD04-147 (E–G), GD04-130 (H) and GD04-190 (J–K), and preserved samples GD04-148 (I) and GD04-149 (L). GD04-147 mylonite contains fine grained shear zones with plagioclase augen crystals (E) and homogeneous monazite crystal (bright phase in the upper centre of the picture, detailed in F) elongate parallel to the shear zone foliation. Monazites also appear associate with hydrated phase as coronae around oxides (G) demonstrating fluid assisted recrystallization process. Monazites from sample GD04-130 (H) and GD04-190 (J–K) are also associated with hydrated phases (mainly biotite). Monazites from preserved granulite samples GD04-148 (I) and GD04-149 (L) are rounded and in equilibrium with plagioclase.

Table 3
$^{40}Ar/^{39}Ar$ dating results of DDU samples.

Step	Laser power (mW)	Atmos pheric conta (%)	^{39}Ar (%)	$^{37}ArCa/^{39}Ar_K$	$^{40}Ar^*/^{39}Ar_K$	Age (Ma ± 1σ)	
GD04-174	**Biotite**						
1	250	11.911	0.12	0.004	34.934	1485.839	±38.91
2	300	0	0.11	75.473	43.892	1728.374	±40.78
3	350	4.429	0.32	0.001	36.181	1521.618	±17.80
4	390	3.758	0.67	0.001	36.341	1526.155	±8.24
5	440	4.373	0.95	–	36.275	1524.283	±5.79
6	500	2.116	2.86	–	36.681	1535.780	±3.36
7	550	1.619	4.8	–	36.766	1538.169	±2.48
8	590	1.737	4.37	–	36.81	1539.388	±2.59
9	640	2.018	5.2	–	36.672	1535.520	±2.36
10	700	0.858	9.45	–	36.686	1535.900	±1.90
11	750	0.767	15.48	–	36.719	1536.827	±1.76
12	780	1.083	10.09	–	36.663	1535.271	±1.85
13	830	0.918	10.76	–	36.794	1538.963	±1.86
14	900	0.904	11.01	–	36.682	1535.799	±1.75
15	1000	0.891	10.78	–	36.715	1536.730	±1.73
16	1150	1.481	6.52	–	36.781	1538.574	±2.06
17	1400	1.507	4.21	–	36.691	1536.046	±1.93
18	2222	2.423	2.29	–	36.887	1541.563	±8.75
GD04-126	**Biotite**						
1	250	5.544	0.87	38.147	28.517	1290.669	±37.70
2	300	5.58	0.86	0.001	36.024	1518.362	±36.37
3	350	3.705	3.04	–	38.126	1577.288	±13.59
4	380	1.301	5.67	–	39.382	1611.578	±6.22
5	400	1.33	5.8	–	39.553	1616.209	±6.56
6	420	0.287	3.74	3.823	39.537	1615.791	±12.72
7	470	2.099	7.45	–	39.574	1616.770	±5.15
8	530	1.636	8.68	–	39.573	1616.760	±4.15
9	600	0.91	15.28	–	39.345	1610.587	±3.22
10	660	1.968	9.38	–	39.493	1614.602	±4.70
11	750	0.966	11.91	–	39.078	1603.350	±3.13
12	840	0.459	8.76	0.258	39.26	1608.297	±6.59
13	1000	1.427	5.49	–	39.336	1610.348	±5.41
14	2222	0.977	13.08	–	39.547	1616.042	±6.21
GD04-120	**Biotite**						
1	250	48.894	1.28	0.004	41.502	1667.227	±40.63
2	300	0	0.6	93.06	47.156	1809.679	±74.35
3	350	9.236	3.1	0.001	35.943	1515.266	±26.29
4	400	2.749	9.71	–	36.058	1518.530	±6.82
5	430	20.869	4.72	0.001	36.137	1520.774	±9.88
6	470	22.633	8.43	–	36.084	1519.286	±7.04
7	510	51.153	3.78	0.001	36.272	1524.607	±12.60
8	580	10.156	6.56	0.001	35.654	1506.985	±9.10
9	700	9.131	19.71	–	35.467	1501.630	±3.91
10	900	6.683	32.76	–	35.676	1507.636	±2.84
11	1100	35.852	6.9	–	35.074	1490.293	±8.48
12	2222	86.827	2.46	0.001	36.298	1525.344	±20.65
GD04-183	**Biotite**						
1	250	53.953	0.17	0.001	25.014	1171.566	±37.03
2	300	29.834	0.15	0.001	35.758	1508.236	±28.74
3	350	5.025	0.91	–	40.398	1636.199	±4.51
4	390	3.037	1.84	–	42.827	1699.750	±3.45
5	420	1.416	3.17	–	42.906	1701.781	±2.29
6	445	1.524	3.14	–	43.04	1705.211	±2.46
7	470	1.034	4.37	–	42.934	1702.495	±1.97
8	490	1.054	2.72	–	42.866	1700.760	±2.50
9	520	0.676	4.14	–	42.941	1702.668	±1.87
10	550	0.785	5.14	–	42.923	1702.223	±2.30
11	580	0.203	4.39	–	42.978	1703.642	±1.98
12	620	0.209	3.88	0.367	42.961	1703.204	±2.26
13	700	0.619	8.52	–	42.962	1703.215	±1.72
14	800	0.493	10.14	–	42.839	1700.056	±1.94
15	890	0.446	11.77	–	42.618	1694.361	±4.40
16	940	0.586	9.69	–	42.763	1698.101	±2.31
17	980	0.818	5.43	–	42.675	1695.842	±2.28
18	1030	0.765	4.35	–	42.797	1698.980	±2.23
19	1100	0.741	3.2	–	42.705	1696.613	±2.59
20	1220	0.813	4.15	–	42.765	1698.170	±1.91
21	2222	0.503	8.73	–	42.821	1699.587	±1.66
GD04-216	**Biotite**						
1	250	46.258	0.48	0.001	29.039	1292.814	±12.75

Table 3 (*Continued*)

Step	Laser power (mW)	Atmos pheric conta (%)	^{39}Ar (%)	$^{37}ArCa/^{39}Ar_K$	$^{40}Ar^*/^{39}Ar_K$	Age (Ma ± 1σ)	
2	300	14.711	0.72	0.001	43.765	1708.934	±8.73
3	340	4.4	3.33	–	43.452	1701.031	±2.93
4	360	4.594	3.25	–	43.358	1698.631	±2.79
5	375	1.813	3.33	–	43.358	1698.644	±4.12
6	395	3.087	4.71	–	43.659	1706.270	±2.58
7	415	2.043	2.27	–	43.274	1696.495	±3.99
8	455	1.188	1.97	–	43.49	1701.977	±3.85
9	540	0.858	5.13	–	43.763	1708.893	±2.30
10	600	0.792	8.14	–	43.934	1713.205	±1.95
11	650	0.618	12.22	–	43.709	1707.516	±2.09
12	685	1.315	7.12	–	43.401	1699.743	±2.23
13	745	2.057	7.1	–	43.474	1701.582	±1.91
14	850	1.706	10.98	–	43.425	1700.348	±1.87
15	960	1.288	15.39	–	43.33	1697.923	±3.00
16	1060	2.141	10.76	–	43.444	1700.815	±2.24
17	1200	5.966	2.17	–	43.263	1696.218	±5.61
18	2222	16.316	0.91	–	43.405	1699.825	±7.90
PMA13	**Biotite**						
1	250	43.941	0.76	0.01	39.811	1622.977	±68.59
2	300	0	1.32	31.364	47.975	1830.107	±33.26
3	350	6.402	5.04	0.001	42.387	1690.937	±11.14
4	400	3.632	12.43	0.001	42.33	1689.450	±6.24
5	440	4.198	8.27	0.001	42.091	1683.239	±8.27
6	500	5.723	5.91	0.001	41.877	1677.678	±12.75
7	580	7.717	5.14	0.001	41.736	1673.998	±11.96
8	700	4.945	10.09	0.001	41.694	1672.885	±7.83
9	900	2.046	26.91	–	41.846	1676.868	±3.30
10	1111	4.841	24.13	–	42.142	1684.574	±3.34
PMA14A	**Biotite**						
1	250	8.764	1.52	0.002	14.796	780.483	±26.15
2	300	22.861	0.69	0.004	35.102	1490.161	±42.10
3	350	3.352	3.39	0.001	42.503	1692.255	±8.72
4	400	3.55	8.07	–	42.017	1679.648	±3.85
5	450	1.815	6.62	–	42.356	1688.451	±5.21
6	500	4.086	5.14	0.001	42.324	1687.624	±4.44
7	570	2.441	14.12	–	43.126	1708.257	±2.94
8	640	1.259	19.38	–	42.838	1700.880	±2.75
9	700	2.786	10.26	–	42.462	1691.196	±3.00
10	780	4.549	8.22	–	42.345	1688.151	±4.11
11	910	1.083	13.73	–	42.309	1687.235	±3.30
12	1060	3.305	5.36	0.001	42.013	1679.542	±6.73
13	2222	4.127	3.5	0.001	42.01	1679.458	±14.34
PMA14C	**Biotite**						
1	250	14.742	2.39	0.001	23.992	1135.360	±16.58
2	300	0.287	2.7	15.688	42.874	1700.107	±13.27
3	350	3.327	7.89	–	41.776	1671.687	±6.73
4	400	2.049	10.58	–	41.834	1673.211	±6.66
5	450	1.067	4.72	3.706	41.893	1674.745	±7.79
6	500	3.278	5.68	–	42.083	1679.700	±6.73
7	570	2.572	13.73	–	42.496	1690.392	±4.86
8	620	1.814	14.24	–	42.103	1680.204	±3.96
9	670	2.548	9.06	–	41.898	1674.874	±4.88
10	740	3.054	5.24	–	41.558	1666.011	±6.73
11	870	0.165	9.89	2.528	41.987	1677.206	±5.28
12	1000	0.196	9.77	3.531	42.135	1681.034	±5.06
13	1220	3.901	2.98	–	40.402	1635.494	±12.89
14	2222	7.02	1.13	0.001	39.517	1611.792	±29.53
AP99-24	**Muscovite**						
1	250	3.42	2.97	–	40.825	1644.411	±5.05
2	280	2.543	3.34	–	42.537	1689.097	±3.30
3	295	0.885	8.92	–	40.584	1638.038	±2.45
4	305	0.761	3.89	–	39.563	1610.749	±3.49
5	315	0.708	23.41	–	39.305	1603.787	±1.65
6	320	2.514	4.16	–	38.499	1581.870	±3.46
7	335	3.937	2.85	–	38.137	1571.928	±3.40
8	400	0.685	43.05	–	38.702	1587.411	±1.49
9	450	0.548	3.88	–	39.726	1615.135	±3.17
10	550	2.849	2.51	–	40.353	1631.885	±2.91
11	750	4.009	0.74	0.001	39.169	1600.115	±15.97
12	2222	12.353	0.28	0.003	37.568	1556.209	±37.61
JJP98-18	**Amphibole**						
1	388.0	66.186	0.04	13.191	26.562	1212.308	±172.305

Table 3 (*Continued*)

Step	Laser power (mW)	Atmos pheric conta (%)	^{39}Ar (%)	$^{37}ArCa/^{39}Ar_K$	$^{40}Ar^*/^{39}Ar_K$	Age (Ma ± 1σ)	
2	442.0	21.377	0.25	2.910	38.532	1571.795	±16.376
3	459.0	–	0.30	1.151	44.088	1717.076	±18.218
4	486.0	–	0.28	1.568	43.221	1695.172	±15.360
5	495.0	–	0.17	2.130	44.337	1723.316	±25.739
6	521.0	0.448	0.54	4.847	45.357	1748.677	±11.157
7	532.0	0.683	0.66	5.896	44.281	1721.915	±12.439
8	551.0	0.029	1.63	6.759	43.781	1709.338	±4.179
9	565.0	–	4.85	7.381	44.034	1715.716	±2.697
10	580.0	–	10.92	7.596	43.790	1709.563	±2.771
11	589.0	–	37.15	7.651	44.298	1722.348	±16.771
12	585.0	–	11.19	7.437	43.717	1707.729	±2.164
13	590.0	–	4.28	7.376	43.867	1711.503	±3.008
14	596.0	–	2.86	7.290	43.696	1707.204	±2.883
15	605.0	–	12.49	7.450	43.776	1709.230	±3.445
16	606.0	–	0.89	7.331	43.631	1705.564	±7.660
17	609.0	–	0.75	6.329	43.612	1705.086	±9.280
18	616.0	–	2.45	7.104	43.912	1712.648	±3.947
19	625.0	–	0.98	6.253	43.484	1701.846	±7.262
20	640.0	0.874	0.43	5.812	42.762	1683.461	±17.184
21	659.0	–	0.87	6.796	44.312	1722.702	±5.631
22	710.0	–	1.70	6.719	44.432	1725.704	±5.597
23	782.0	–	0.43	6.850	45.545	1753.303	±12.498
24	881.0	–	1.89	6.593	46.709	1781.747	±4.133
25	980.0	–	1.99	8.028	44.362	1723.950	±5.162
JJP98-18	**Biotite**						
1	353.0	15.817	0.12	–	52.233	1910.892	±175.032
2	372.0	8.407	0.33	–	48.094	1815.007	±54.250
3	398.0	3.220	0.69	0.024	43.771	1709.100	±19.040
4	422.0	0.707	1.31	0.016	43.590	1704.524	±10.726
5	444.0	0.116	3.15	0.002	42.869	1686.178	±6.277
6	466.0	0.561	4.42	–	42.448	1675.397	±4.527
7	494.0	–	3.65	––	42.637	1680.254	±5.756
8	526.0	–	2.97	–	42.765	1683.534	±6.224
9	556.0	–	9.21	0.002	42.407	1674.352	±2.724
10	580.0	0.206	7.48	–	42.151	1667.749	±3.492
11	610.0	–	14.86	–	42.047	1665.054	±2.192
12	628.0	0.421	8.09	0.002	42.063	1665.477	±3.012
13	675.0	–	11.07	–	42.215	1669.390	±3.341
14	717.0	–	12.55	–	42.354	1672.975	±4.004
15	755.0	–	15.21	0.003	42.092	1666.206	±2.325
16	786.0	0.168	3.22	0.004	42.346	1672.760	±6.348
17	827.0	1.192	1.04	–	42.378	1673.602	±15.805
18	900.0	1.018	0.64	0.029	43.154	1693.452	±24.613
JJP98-17	**Amphibole**						
1	365.0	14.229	0.02	9.325	72.884	2325.387	±280.793
2	379.0	15.475	0.01	7.002	48.324	1820.483	±347.986
3	394.0	–	0.02	7.272	62.727	2133.375	±240.383
4	426.0	–	0.01	25.483	219.190	3945.106	±406.027
5	441.0	–	0.25	7.001	53.543	1940.216	±26.561
6	455.0	1.811	0.36	6.894	45.538	1753.150	±19.969
7	469.0	–	5.92	6.790	43.688	1706.990	±2.733
8	474.0	–	3.48	6.861	43.396	1699.612	±3.335
9	479.0	–	3.22	6.833	43.426	1700.361	±3.316
10	484.0	–	8.36	6.929	43.467	1701.395	±2.800
11	490.0	–	0.45	6.985	43.975	1714.223	±13.048
12	502.0	–	1.04	6.939	43.941	1713.364	±8.540
13	509.0	–	1.59	6.884	43.698	1707.261	±6.331
14	520.0	–	3.05	6.796	43.612	1705.083	±2.724
15	530.0	–	9.36	6.789	43.414	1700.053	±2.774
16	535.0	–	3.48	6.786	43.358	1698.642	±3.743
17	541.0	–	3.58	6.801	43.328	1697.882	±3.321
18	547.0	–	3.62	6.855	43.648	1705.994	±2.992
19	554.0	–	8.74	6.755	43.407	1699.892	±3.806
20	560.0	–	2.39	6.764	43.458	1701.169	±4.511
21	565.0	–	2.95	6.748	43.373	1699.023	±3.979
22	570.0	–	6.05	6.718	43.690	1707.058	±7.738
23	571.0	–	6.36	6.789	43.484	1701.836	±2.483
24	576.0	–	5.78	6.754	43.415	1700.095	±2.424
25	581.0	–	2.79	6.712	43.525	1702.862	±4.433
26	588.0	–	7.18	6.748	43.435	1700.597	±2.193
27	596.0	–	2.24	6.852	43.497	1702.153	±4.783
28	612.0	0.530	0.57	6.920	43.254	1696.007	±13.817
29	641.0	–	3.14	6.676	43.719	1707.776	±3.347
30	672.0	–	0.25	6.859	46.852	1785.202	±39.735

Table 3 (*Continued*)

Step	Laser power (mW)	Atmos pheric conta (%)	^{39}Ar (%)	$^{37}ArCa/^{39}Ar_K$	$^{40}Ar^*/^{39}Ar_K$	Age (Ma ± 1σ)	
31	762.0	–	2.97	6.777	44.014	1715.217	±3.217
32	800.0	0.597	0.80	6.953	43.745	1708.435	±9.435
JJP98-17	**Biotite**						
1	339.0	1.605	1.02	–	49.172	1840.479	±23.826
2	356.0	–	4.10	0.015	44.342	1723.433	±6.317
3	374.0	–	6.54	0.008	43.810	1710.067	±4.402
4	392.0	–	7.97	0.012	43.922	1712.891	±3.241
5	412.0	–	4.48	0.007	43.736	1708.220	±6.878
6	432.0	0.354	5.07	0.026	43.298	1697.126	±5.103
7	455.0	0.177	14.39	0.009	42.424	1674.785	±4.312
8	477.0	0.074	12.08	0.013	42.525	1677.366	±3.298
9	497.0	0.234	7.52	0.012	42.370	1673.382	±4.085
10	519.0	0.115	6.69	0.022	42.515	1677.117	±4.778
11	538.0	–	7.77	0.013	42.631	1680.095	±4.702
12	558.0	–	4.19	0.028	43.279	1696.642	±7.623
13	577.0	0.141	9.90	0.015	42.526	1677.399	±4.187
14	596.0	0.381	2.58	0.049	42.963	1688.587	±10.254
15	620.0	1.272	3.43	0.026	42.221	1669.537	±8.406
16	645.0	–	1.80	–	42.647	1680.509	±11.860
17	676.0	5.387	0.20	0.164	42.790	1684.173	±108.002
18	1550.0	–	0.28	–	43.596	1704.672	±63.996
JJP98-6	**Amphibole**						
1	434.0	4.852	0.20	5.598	114.756	2953.147	±21.071
2	464.0	–	45.20	5.705	43.414	1700.067	±13.968
3	469.0	–	27.05	5.738	43.825	1710.451	±29.243
4	473.0	–	3.65	5.774	43.485	1701.857	±3.744
5	455.0	–	23.89	5.655	43.635	1705.650	±27.813
JJP98-6	**Biotite**						
1	322.0	2.401	3.00	0.022	43.938	1713.299	±5.321
2	343.0	0.009	4.98	0.008	43.087	1691.761	±4.158
3	363.0	–	8.60	0.002	42.991	1689.292	±2.830
4	384.0	0.046	8.67	0.002	42.488	1676.412	±2.672
5	403.0	0.123	6.88	0.011	42.389	1673.868	±3.575
6	445.0	0.030	8.14	0.009	42.004	1663.938	±3.052
7	465.0	0.152	14.95	0.004	41.648	1654.715	±3.207
8	486.0	0.494	1.77	0.016	41.303	1645.726	±8.771
9	511.0	1.146	3.97	0.038	40.894	1634.989	±4.829
10	535.0	0.054	4.07	0.010	41.667	1655.213	±3.563
11	555.0	0.053	8.50	0.004	41.536	1651.796	±3.255
12	575.0	0.048	5.06	0.003	41.906	1661.416	±4.066
13	595.0	–	4.43	0.007	42.137	1667.384	±3.800
14	616.0	–	3.05	0.015	42.296	1671.484	±5.859
15	636.0	–	10.27	0.010	41.839	1659.661	±2.622
16	658.0	–	3.65	–	41.722	1656.644	±6.497
AP99-36	**Amphibole**						
1	368.0	23.380	0.11	40.283	85.614	2540.317	±40.133
2	420.0	5.219	0.30	7.118	48.296	1819.797	±18.937
3	458.0	0.842	0.78	3.200	42.914	1687.324	±7.544
4	475.0	–	0.43	3.840	41.951	1662.582	±15.431
5	469.0	–	0.42	5.251	43.575	1704.127	±14.557
6	480.0	–	0.59	6.503	43.287	1696.828	±15.646
7	484.0	0.258	0.88	7.089	42.980	1689.032	±10.756
8	487.0	0.295	1.63	7.020	42.516	1677.143	±4.718
9	498.0	–	5.68	6.818	42.312	1671.885	±2.422
10	502.0	–	7.18	6.655	42.281	1671.088	±2.065
11	508.0	–	2.33	6.489	42.248	1670.251	±3.902
12	514.0	–	3.79	6.506	42.331	1672.380	±3.086
13	519.0	–	8.67	6.546	42.394	1674.007	±2.575
14	522.0	–	6.43	6.532	42.284	1671.183	±2.590
15	523.0	–	2.78	6.485	42.202	1669.051	±3.094
16	526.0	–	1.40	6.529	42.785	1684.039	±7.148
17	532.0	–	5.17	6.493	42.499	1676.697	±3.975
18	538.0	–	2.84	6.523	42.886	1686.633	±9.910
19	520.0	–	7.53	6.455	42.327	1672.280	±3.071
20	538.0	–	1.70	6.145	42.806	1684.579	±4.513
21	549.0	–	5.65	6.393	42.499	1676.699	±2.762
22	560.0	–	14.28	6.461	42.403	1674.249	±1.972
23	563.0	–	2.51	5.996	42.165	1668.102	±4.001
24	568.0	–	1.94	5.819	42.294	1671.427	±4.664
25	570.0	–	0.48	14.690	44.027	1715.544	±16.130
26	583.0	–	0.47	6.768	42.421	1674.692	±13.672
27	613.0	–	0.33	10.773	43.784	1709.428	±18.782

Table 3 (*Continued*)

Step	Laser power (mW)	Atmos pheric conta (%)	^{39}Ar (%)	^{37}ArCa/^{39}Ar$_K$	^{40}Ar*/^{39}Ar$_K$	Age (Ma ± 1σ)	
28	647.0	–	1.12	6.980	42.258	1670.510	±7.272
29	694.0	–	2.87	6.951	42.495	1676.612	±3.019
30	770.0	–	1.92	4.905	41.932	1662.082	±4.468
31	810.0	–	7.79	5.025	42.588	1678.996	±1.875
JJP98-4	**Biotite**						
1	335.0	–	0.08	–	57.953	2035.550	±225.017
2	353.0	–	1.24	–	44.797	1734.793	±16.018
3	370.0	–	0.31	0.070	43.603	1704.838	±53.241
4	402.0	0.788	1.79	–	41.010	1638.051	±9.199
5	423.0	0.474	3.72	0.019	41.111	1640.682	±5.381
6	444.0	–	5.30	0.024	40.991	1637.546	±3.737
7	464.0	0.052	4.54	0.020	40.803	1632.603	±4.899
8	494.0	–	7.46	0.008	40.562	1626.235	±3.021
9	523.0	0.043	8.36	0.007	40.476	1623.969	±3.174
10	555.0	0.362	9.58	0.005	40.064	1613.045	±3.048
11	585.0	0.089	24.26	0.002	40.250	1617.990	±1.996
12	599.0	1.770	1.51	0.011	39.587	1600.301	±11.879
13	631.0	0.091	4.83	0.003	40.238	1617.669	±4.345
14	660.0	0.392	5.60	–	40.218	1617.120	±4.058
15	696.0	–	8.42	–	40.385	1621.554	±3.793
16	724.0	0.485	3.97	–	40.353	1620.703	±5.374
17	782.0	–	5.64	0.008	40.156	1615.471	±4.119
18	940.0	–	1.51	–	40.126	1614.679	±14.777
19	1111.0	–	1.88	0.009	40.651	1628.596	±10.361
OM110-1	**Biotite**						
1	326.0	1.809	2.11	0.016	40.456	1623.431	±23.664
2	346.0	13.392	0.20	0.282	40.474	1623.914	±199.643
3	376.0	0.514	16.41	0.008	39.424	1595.916	±4.290
4	398.0	0.076	12.81	0.007	38.854	1580.532	±5.706
5	420.0	0.139	7.21	0.001	38.937	1582.799	±7.171
6	450.0	0.352	5.84	0.015	38.957	1583.332	±9.710
7	488.0	–	5.72	0.000	38.595	1573.504	±6.363
8	535.0	–	16.17	0.015	38.824	1579.720	±4.098
9	581.0	–	15.18	0.011	38.915	1582.193	±3.130
10	622.0	–	10.70	–	38.927	1582.530	±5.793
11	663.0	–	3.98	–	39.160	1588.814	±16.695
12	723.0	–	3.67	–	39.030	1585.300	±11.355
DDU89	**Muscovite**						
1	327.0	1.809	32.15	0.013	40.313	1619.646	±4.216
2	328.0	0.935	10.26	0.051	39.234	1590.799	±9.845
3	332.0	1.786	5.51	0.104	39.502	1598.006	±18.031
4	342.0	0.295	45.95	0.006	39.217	1590.344	±3.859
5	348.0	0.601	6.13	0.063	39.221	1590.456	±14.453

from the narrow shear zones within the Neoarchaean crust, monazite ages from mylonitic gneiss at Aurora Peak, adjacent to the MSZ, record a slightly younger age at 1619 ± 48 Ma (MSWD 0.97, n = 10).

In the Neoarchaean granulite crust, ^{40}Ar/^{39}Ar analyses of biotites (Fig. 5) display rather flat age spectra allowing plateau age calculations in the range 1509 ± 3 Ma (sample GD04-120, Stillwell Island) to 1702 ± 3 Ma (GD04-183, Cape Gray), with intermediate plateau ages at 1537 ± 3 Ma (sample GD04-174, Close Island) and 1612 ± 3 Ma (sample GD04-126, Cape Pigeon).

4.1.2. The western amphibolite Neoarchaean crust

In comparison with biotites from the granulite crust, ^{40}Ar/^{39}Ar analyses of biotites from the amphibolite crust (Fig. 6) display slightly disturbed age spectra with slight humped shapes, with the exception of sample PMA13. Such hump shapes indicate a slight chloritization of the biotites (Ruffet et al., 1991). These authors suggest that the high temperature pseudo-plateau ages could be the best estimates of the true ages of the analysed biotites. Calculated plateau and pseudo-plateau ages are globally older and less scattered than ^{40}Ar/^{39}Ar biotite ages from granulitic domain. They range between 1678 ± 3 Ma (PMA14C, Port Martin) and 1700 ± 3 Ma in (GD04-216, Cap de la Découverte), with intermediate ages at 1681 ± 3 Ma (PMA13, Port Martin) and 1687 ± 3 Ma also in Port Martin (PMA14A, Fig. 8E).

4.2. Paleoproterozoic basins

4.2.1. The Cape Hunter basin

^{40}Ar/^{39}Ar dating of a muscovite (AP99-24, Fig. 7) from the Cape Hunter phyllite (Fig. 8D) yields a saddle shaped age spectrum. Such an age spectrum for a single grain of muscovite has been interpreted to reflect the mixing of two age components, an inherited or initial mineral phase and a recrystallized or neocrystallized phase, which may or may not be linked to deformation (Cheilletz et al., 1999; Castonguay et al., 2001; Alexandrov et al., 2002). The saddle-shaped age spectrum results from the existence of different reservoirs with distinct argon compositions in the partially recrystallized muscovite grains, with "shifted" argon degassing of a primary unrecrystallized domain and a neo- or re-crystallized one. This younger neo- or re-crystallized subdomain indicates either a thermal event, at or younger than 1589 ± 3 Ma, unrelated to the crystallization of the initial muscovite which occurred at or prior to *ca.* 1640 Ma, or the last isotopic record of a protracted (re)crystallization history during slow cooling, between 1640 Ma and 1589 Ma.

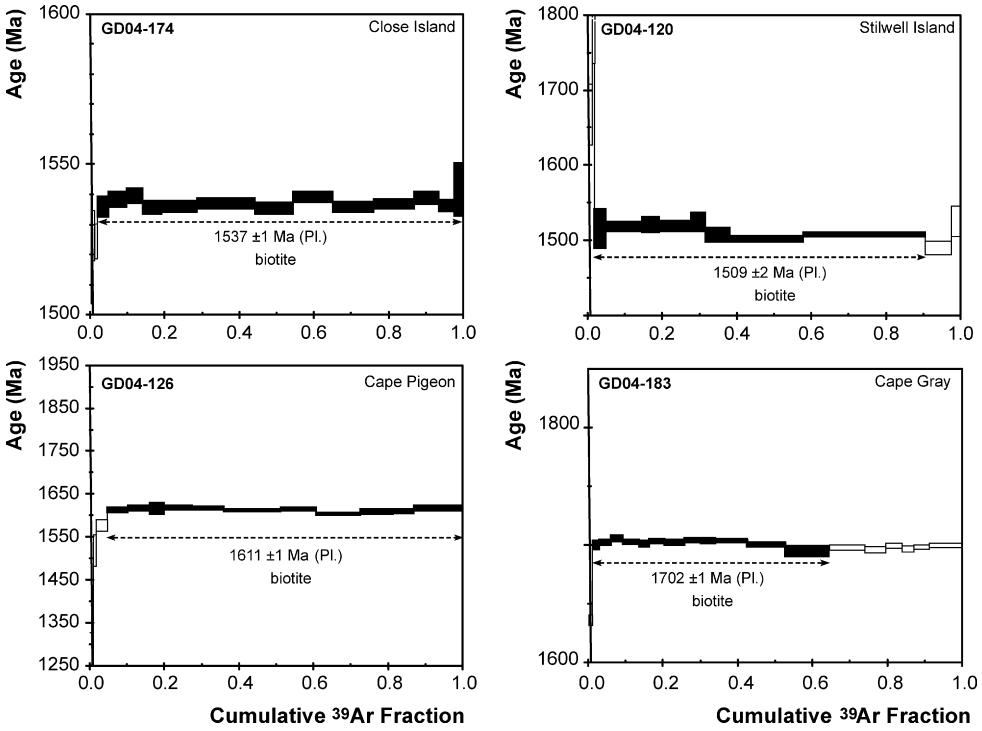

Fig. 5. Argon spectra for the Deep Neoarchaean crust.

4.2.2. The Dumont D'Urville basin

In the eastern region of the Dumont D'Urville basin, Cap Jules samples exhibit $^{40}Ar/^{39}Ar$ plateau ages in all analysed amphibole and biotite samples (Fig. 7). Biotite ages range between 1643 ± 3 Ma (JJP98-6) and 1664 ± 3 Ma (JJP98-17), with an intermediate age of 1654 ± 3 Ma (sample JJP98-18). Amphibole ages range between 1678 ± 3 Ma (JJP98-17) and 1691 ± 7 Ma (JJP98-18), with an intermediate age of 1682 ± 12 Ma (JJP98-6).

Further west, the Cap Bienvenüe biotite sample displays (Fig. 7) a pseudo-plateau age of 1606 ± 3 Ma (JJP98-4). Amphibole from the same locality records a plateau age of 1651 ± 3 Ma (AP99-36).

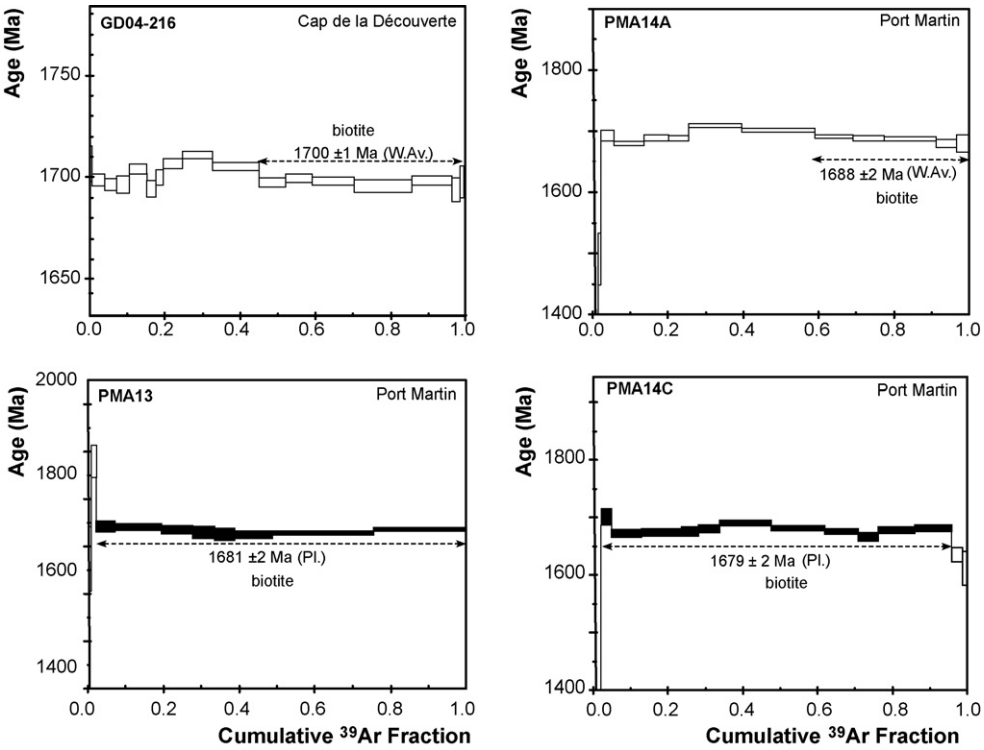

Fig. 6. Argon spectra for the Intermediate to upper Neoarchaean crust.

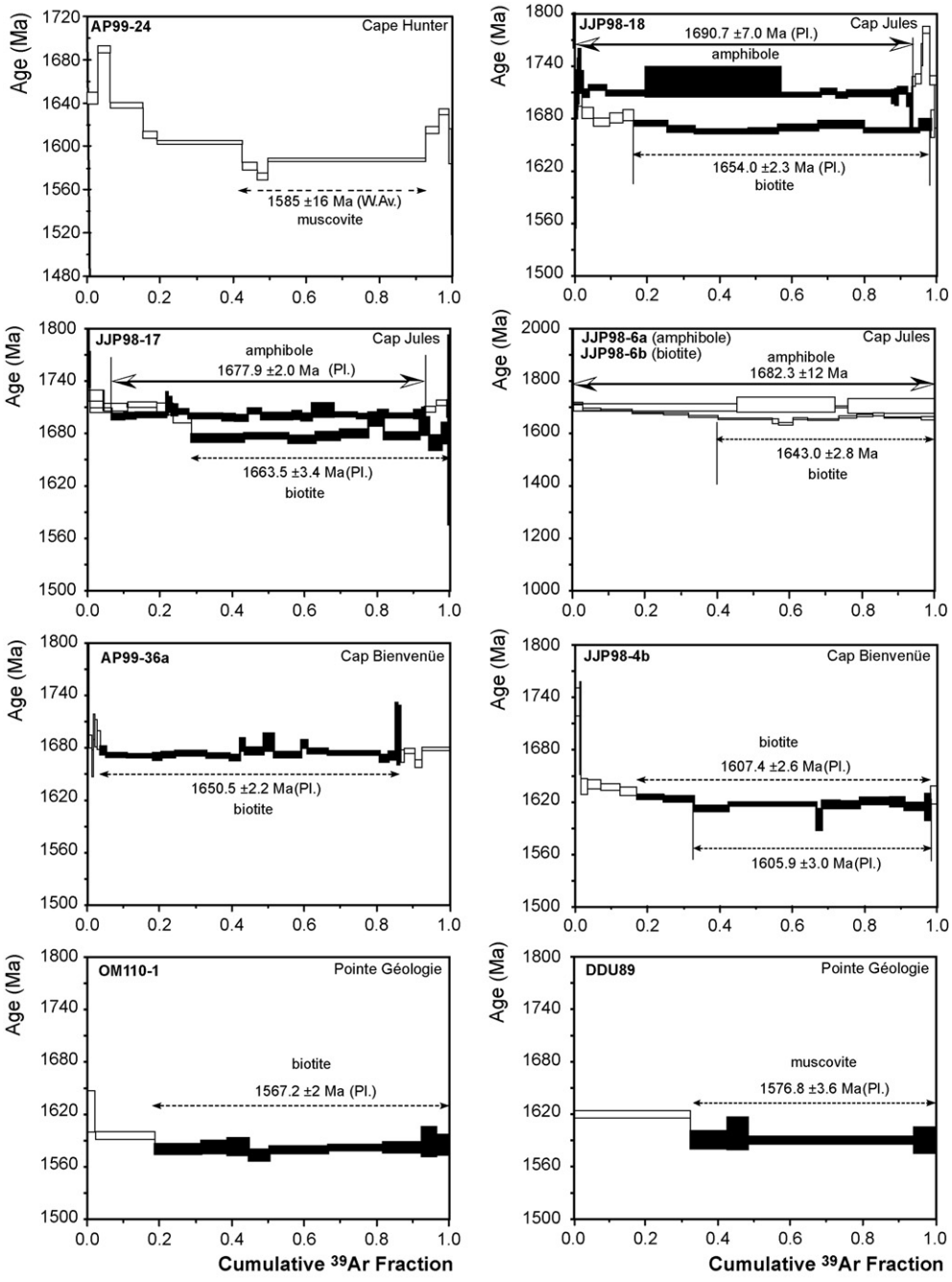

Fig. 7. Argon spectra for the Paleoproterozoic basins.

Finally, Pointe Géologie samples (Fig. 7) yield a plateau age of 1567.2 ± 2.2 Ma (biotite OM110-1) and a pseudo-plateau age of 1576.8 ± 3.6 Ma (muscovite DDU89).

This clearly points out decreasing plateau ages from East to West in the Dumont d'Urville basin, *i.e.* from Cap Jules towards Pointe Géologie (Fig. 9).

5. Discussion

In the following section, we interpret the new Th–U–Pb and $^{40}Ar/^{39}Ar$ geochronological data presented above together with previously published ages (Peucat et al., 1999a,b; Oliver and Fanning, 2002; Di Vincenzo et al., 2007). The aim of this discussion is to outline the tectonic history and geodynamic evolution of the TAC's different domains. Scattered ages seem to indicate a three-step tectonic history reworking a 2.8–2.6 Ga juvenile crust.

5.1. Significance of the Th–U–Pb monazite and U–Pb zircon data

5.1.1. The Neoarchaean crust

Monazite analyses from the deep Neoarchaean crust illustrate a complex and polyphase tectonic and metamorphic evolution with two major events, occasional inheritance, and partial resetting.

Monazites from preserved granulite and amphibolite facies rocks record a major tectonothermal event between 2477 Ma and 2433 Ma. Peucat et al. (1999b) and Oliver and Fanning (2002) also record U–Pb SHRIMP ages around 2.44 Ga in the grey gneisses of

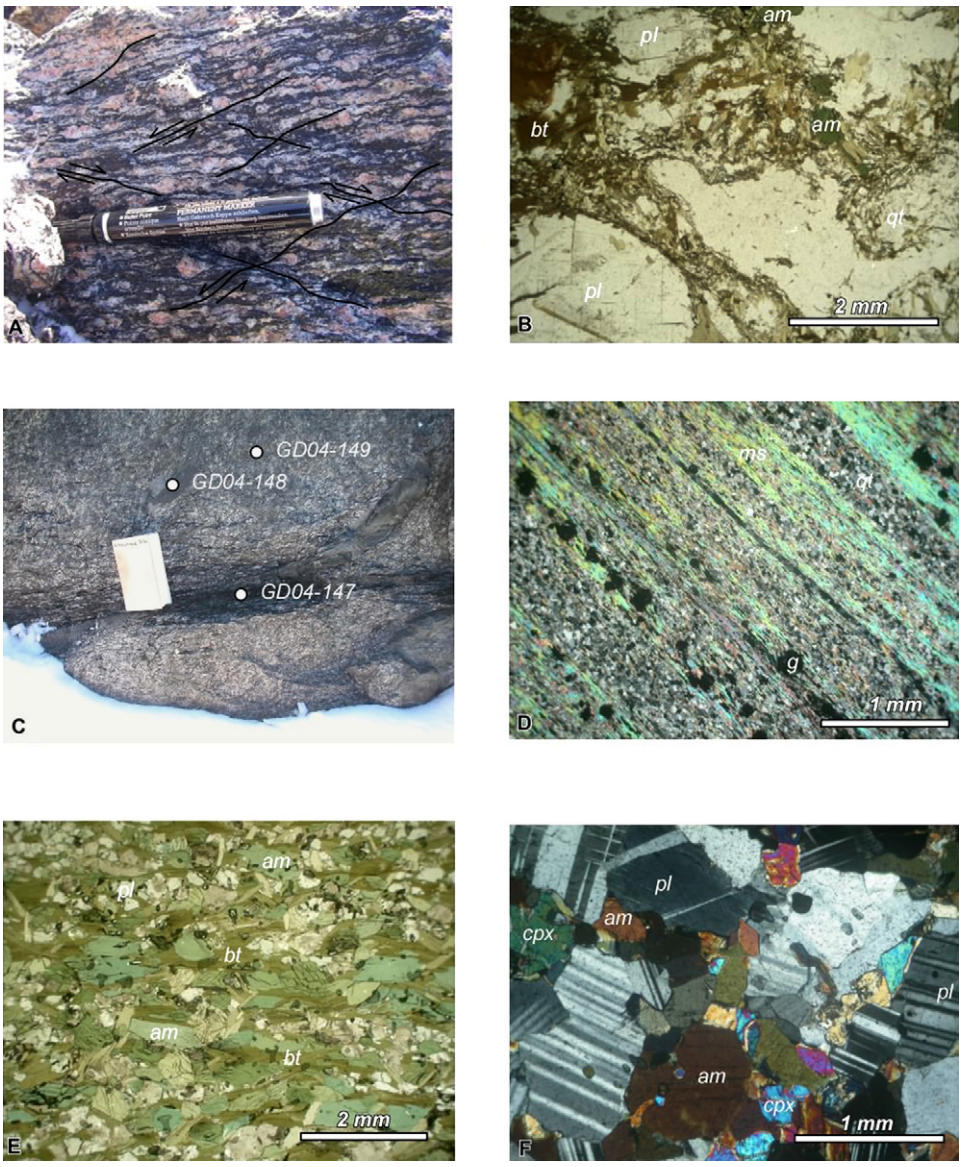

Fig. 8. Photography plate. (A and B) Strained and meta-granodiorites from Correll Nunatak recrystallized under greenschist facies conditions. Image A illustrates the conjugate senses of shear observed on the Mertz Shear zone; Image B shows the replacement of amphibole by biotite along shear zones; (C) C Island samples relationship underlining the small scale 1.7 Ga resetting along narrow shear zones within the Neoarchaean crust (see text for details); (D) Microscope view of the Cape Hunter phyllite. A primary stratification remains recognisable, underlined by qt-rich and ms-rich layers alternation. (E) Port Martin mafic xenolith (PMA14A) illustrating the static retrogression of amphiboles in green biotite; (F) Syntectonic gabbro from the Cap Jules (JJP98-17) illustrating the preservation of magmatic fabric.

the Port Martin and Cape Denison. This age range is interpreted to be the age of the HT granulite facies metamorphism and of subsequent migmatization during granulite to amphibolite facies retrogression associated with decompression around 2.45–2.43 Ga (Duclaux, 2007).

Rounded monazites included in plagioclase from sample GD04-148, (a mafic xenolith, Fig. 3A and I) and from sample GD04-124 (an anatectic granite) display age populations of *ca.* 2.63 Ga and *ca.* 2.59 Ga respectively. Further west, in the intermediate to upper amphibolitic crustal Neoarchaean subdomain, inherited zircons have also been dated by Peucat et al. (1999b) between 2.7 Ga and 2.6 Ga. Moreover, these authors have interpreted Nd model ages from grey gneiss between 2.6 Ga and 2.8 Ga to be associated to a previous period of major continental crust genesis.

The second major event is defined by the 1696–1712 Ma population ages. These ages are found throughout the granulite crust, but localized within decimetre to metre scale shear zones. This is well exemplified on C Island (Figs. 3C, E–G and 8C), where GD04-147 (shear zone: 1696 Ma) and GD04-149 (isotropic granulitic tonalite: 2433 Ma) samples are separated by only a few metres. In this case neither the isotropic tonalite sample, nor the xenoliths record any latter resetting. A zircon SHRIMP U–Pb age at 1.70 Ga has also been obtained by Oliver and Fanning (2002) in a sheared Neoarchaean orthopyroxene bearing mafic gneiss from Madigan Nunatak, south of Cape Denison.

The population age between 2.2 Ga and 1.82 Ga is not easily interpreted in terms of tectonic reactivation. Monazites dated in this age range are poorer in ThO_2 (here <3 wt%, see Table 2), which seems to be symptomatic of low temperature reequilibration (Wing et al., 2003; Finger and Krenn, 2007). They might have crystallized directly from a fluid as crystals lie within the rocks' foliation associated with hydrated phases (Fig. 3). Furthermore, in Fig. 4, the richest PbO monazites from mylonitic samples GD04-190

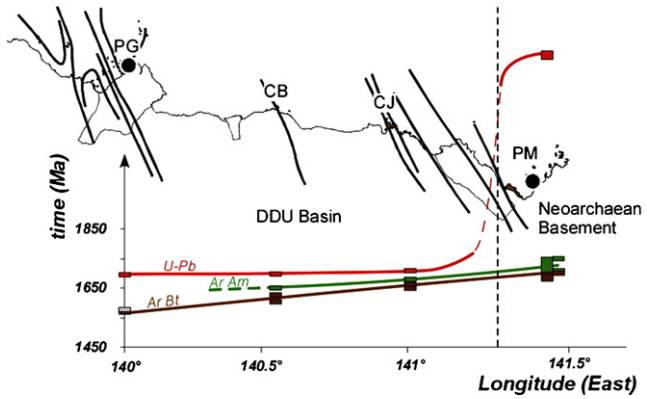

Fig. 9. Longitudinal time–temperature projection in the Dumont D'Urville basin and its eastern basement, sub-perpendicular to the regional foliation strike (black curves). Red, green, grey and brown boxes correspond to zircon or monazite U–Pb (closure temperature ~700 °C), Amphibole Argon (~550 °C), Muscovite Argon (~450 °C) and Biotite Argon (~350 °C) ages respectively. Lines divergence from Port Martin to Point Géologie illustrates an exhumation gradient from east to west, with exhumation rates up to 0.2 mm yr^{-1} in Cape Jules decreasing westward to 0.1 mm yr^{-1}. This exhumation gradient correlates with the deformation gradient from dome-shaped structures to the west to vertical shear zones to the east described by Pelletier et al. (2002). Abbreviations for localizations are the same than in Fig. 2. (For interpretation of the references to colour in this figure legend, the reader is referred to the web version of the article.)

and GD04-130 are above the 1.7 Ga line. Other monazite analyses from these samples lie on the 1.7 Ga curve for $ThO_2{}^* < 4.5$ and 6.5 respectively, supporting age mixing and partial resetting during the *ca.* 1.7 Ga event. Pb loss cannot be directly inferred by the electron probe technique and would require isotopic analysis to be established. Carbonate bearing metapelites GD04-155 and retromorphosed granulite RPM03-37, associated with marbles and calc-silicates, record age inheritance at *ca.* 2090 Ma, supporting that the Moyes archipelago's metasediments belong to the Neoarchaean domain as they record a high-grade metamorphic imprint prior to 2.0 Ga.

As suggested by Oliver and Fanning (2002) in relation to Madigan Nunatak and new data from Cape Gray (GD04-190) or Watt Bay (GD04-130 and GD04-147), the 1.7 Ga tectonic reactivation localized in shear zones marked by ultramylonites under low grade conditions is associated with fluid circulation (Fig. 3C–H, J and K). Here, it is evident that the transition zone between the granulite and the amphibolite subdomains may define a major rheological boundary within the Neoarchaean crust.

5.1.2. The Paleoproterozoic basins

In the Paleoproterozoic domain, published U–Pb ages from Peucat et al. (1999a) for the Dumont D'Urville Basin migmatites range between 1712 ± 7 Ma (zircon from sample JJP98-6) and 1695 ± 5 Ma (monazite from sample OM110-1). These enable us to define the regional metamorphic peak at 1700 ± 10 Ma all over the basin.

5.2. Significance of the $^{40}Ar/^{39}Ar$ data

5.2.1. The Neoarchaean granulite crust

On the eastern margin of the TAC, within the Mertz shear zone, Di Vicenzo et al. (2007) have obtained $^{40}Ar/^{39}Ar$ laserprobe biotite ages ranging from 1492 ± 11 Ma to 1559 ± 08 Ma at the Corell Nunatak (in the amphibolitic crust along the Mertz Shear zone—Fig. 8A and B) and 1502 ± 09 Ma at the Aurora Peak (in granulite facies). We obtained biotite plateau ages in a similar range: 1509 ± 03 Ma at Stillwell Island and 1537 ± 03 Ma on Close Island. These results support the occurrence of a thermal event along the Mertz shear zone during the ~1500–1550 Ma time range.

In contrast, the much older biotite plateau age of 1702 ± 03 Ma (GD04-183) in the Cape Gray, tens of kilometres to the West, indicates that the 1500–1550 Ma thermal overprinting or extensive fluid flow + deformation event is localized and not pervasive within the rest of the craton.

The biotite age from the Cape Pigeon shear zone sample (GD04-126) lies in between these two age groups. It is older (~1612 Ma) than the ~1.50–1.55 Ga age range. This latter age is interpreted as being due to excess ^{40}Ar as biotite can be a sink of excess ^{40}Ar during fluid circulation within a shear zone (e.g., Arnaud and Kelley, 1995). In the Cape Pigeon case, excess ^{40}Ar is not apparent from the data plots alone, as the biotite $^{40}Ar/^{39}Ar$ spectra show flat plateau ages, and the inverse isochron plots preserve an atmospheric initial ratio of $(^{36}Ar/^{40}Ar)_0$. However, even in cases of flat Ar spectra, biotite dating has shown to yield unrealistic geological ages especially in cases of mylonitic deformation (Leloup et al., 2005; Rolland et al., 2007, 2008). As the biotite sample GD 04-126 was sampled in a mylonite, it is likely that its slightly older age may be due to some excess ^{40}Ar, although this excess component is not visible from the $^{36}Ar/^{40}Ar$ vs $^{39}Ar/^{40}Ar$ isochron plots. This excess component may be inherited from 1.7 Ga relic minerals.

In contrast to the biotite $^{40}Ar/^{39}Ar$ data, which show plateau or mini-plateau ages in almost all samples, amphibole $^{40}Ar/^{39}Ar$ data from Di Vicenzo et al. (2007) show highly disturbed spectra. Indeed, their $^{40}Ar/^{39}Ar$ laserprobe apparent ages range from 1722 Ma to 2402 Ma. Di Vincenzo et al. interpreted the variations older than 1.7 Ga as reflecting the presence of excess ^{40}Ar in the analysed samples, which could be ascribed to other mineral inclusions such as clinopyroxene. They further ascribe the ~1.7 Ga ages as reflecting a "real" tectonometamorphic event. Moreover, the 1.50–1.55 Ga event has not totally reset the $^{40}Ar/^{39}Ar$ amphibole chronometer as older ages of 1.7 Ga and >1.9 Ga are obtained (Di Vincenzo et al., 2007). Thus this late 1.50–1.55 Ga thermal resetting seems to have occurred under low temperature conditions, not exceeding amphibole closure temperature (<500 °C).

5.2.2. The Neoarchaean amphibolite crust

Biotite samples exhibit plateau ages between 1678 ± 03 Ma (Port Martin) and 1700 ± 03 Ma (Cap de la Découverte). Some samples show only a mini-plateau age in agreement with other plateau ages. This is due to a small disturbance in the low temperature part of the spectra (Port Martin and Cap de la Découverte samples). We interpret this low temperature disturbance as resulting from a short-lived thermal event close to the closure temperature of the Ar system in biotite (300–350 °C—Harrison et al., 1985). This short-lived event may result from late fluid flow along the shear zones and is likely to be contemporaneous the ~1500 Ma event as it is well developed close to the MSZ.

5.2.3. The Paleoproterozoic basins

In the Dumont D'Urville Basin, all biotite samples show plateau ages (Fig. 7). The plateau ages range between 1567.2 ± 2.2 Ma (Pointe Géologie) and 1690.7 ± 7.0 Ma (Cap Jules). Furthermore, the $^{40}Ar/^{39}Ar$ data evidence a space and time gradient, with decreasing ages from East to West, as already noted for amphibole ages. In contrast, U–Pb ages for both Pointe Géologie and Cap Jules are similar (data from Peucat et al., 1999a; Pelletier et al., 2002 and unpublished data). Consequently, we interpret the lateral $^{40}Ar/^{39}Ar$ biotite age gradient as reflecting a variation in the exhumation rate. According to the *P–T* estimates of Pelletier et al. (2002), a geothermal gradient of 35 °C km^{-1} is inferred and for an average crustal

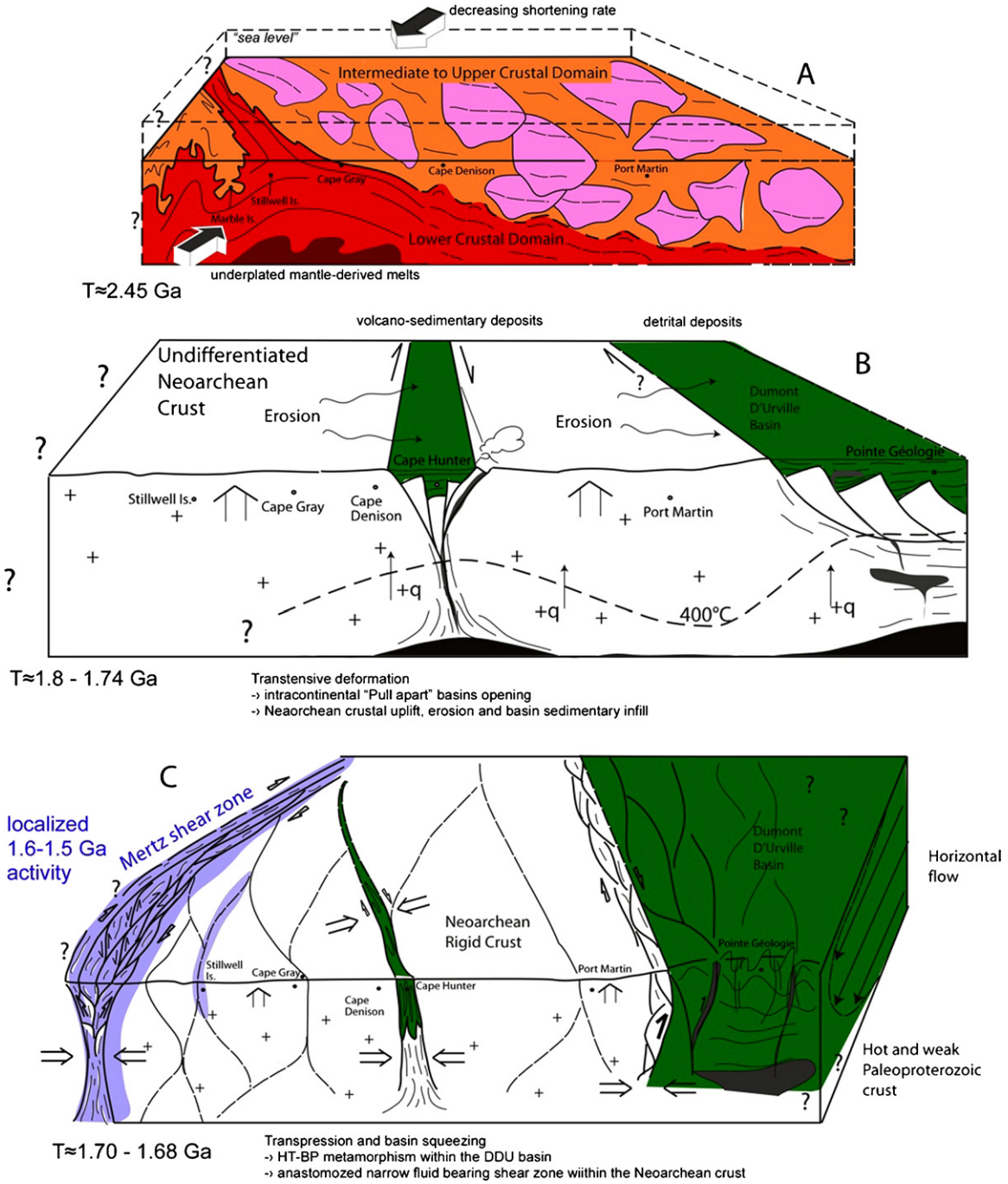

Fig. 10. Geodynamic evolution sketch. Geodynamic evolution sketch of the TAC in Late Archaean to Proterozoic times (view is towards the south). (A) The main Eastern TAC orogenic event major occurred at 2.45 Ga in a NE–SW shortening context. This tectono-thermal event reactivated the 2.8–2.6 Ga juvenile crust of the TAC. In red, the deep crust is metamorphosed under granulite facies metamorphism associated with mafic underplating (brown colour). This is directly followed by retrogression under amphibolite facies conditions and important partial melting and granodioritic magmas emplacement around 2450 Ma. Important lateral flow of the crust favored thinning and acquisition of a dome-shaped structure exhumating the granulitic crustal root. (B) Continuous uplift of this Late Archaean crust is allowed by mechanical erosion and trans-current basins opening (Cape Hunter and Dumont D'Urville, in green). These processes favored recycling Neoarchaean material before 1.76 Ga. Basins were filled with detrital material from the surrounding basement in addition to some newly formed magmas. (C) Tectonic convergence and basins closure occurred around 1.7 Ga. Basins were squeezed. The DDU basin records HT-LP metamorphism associated with anatexis. Dome structures developed in the central part of the basin and vertical shear zones concentrated to the east, at the contact with the cold and strong Neoarchaean crust. This latter domain acted as a rigid block and developed narrow anastomosed shear zones acting as a plumbing system for fluid circulations. Deformation along the Mertz Shear zone (purple colour) seems to initiate at c. 1.62 Ga, and to remain active until around 1.51 Ga as shown by Ar–Ar data. (For interpretation of the references to colour in this figure legend, the reader is referred to the web version of the article.)

density of 2.7, we estimate slow and slightly dissimilar exhumation rates of 0.2 ± 0.5 mm yr^{-1} in the east and 0.1 ± 0.5 mm yr^{-1} in the west.

Muscovite ages are similar within error in the Cape Hunter phyllites (maximum age of 1585 ± 16 Ma) and in the Pointe Géologie migmatites (1576.8 ± 3.6 Ma, mini-plateau age). As Pointe Géologie muscovite is ~9 Ma older than biotite from the same sample, it suggests a cooling rate of 6 ± 2 °C Ma^{-1} estimated from the T–t history based on U–Pb ages on monazites and ^{40}Ar/^{39}Ar ages on biotites (and closure temperatures by Harrison et al., 1985).

5.3. Tectonic history

According to the published structural data (Ménot et al., 2005; Duclaux et al., 2007) and geochronological data (Oliver and Fanning, 1997; Peucat et al., 1999b; Di Vincenzo et al., 2007; this study), we put forward a tectonic history of the TAC from the Neoarchaean to the Mesoproterozoic. Further, the tectonic evolution, inferred from structural and geochronological data is summarized in Fig. 10 and can be separated into four tectonic phases:

(1) The Neoarchaean phase: A 2.6–2.8 Ga juvenile continental crust is metamorphosed under HT granulite to amphibolite facies conditions at around 2.47 Ga. In the eastern TAC, a deep crustal granulite domain is exhumed in a dome-shaped structure and deformation is dominated by horizontal constriction. Evidence for this vertical motions is the occurrence of narrow upper-crustal sedimentary derived rock pods (*i.e.* in the Moyes Archipelago) that have recrystallized under granulite facies conditions (Fig. 10A). These observations are in agreement with the models of Cagnard et al. (2006), suggesting both vertical and horizontal ductile flow of the weak and warm lower crust. Such weakening of the lower crust can be explained by the underplating of large volumes of mantle-derived melts as proposed within the Dharwar craton by Chardon et al. (2002). Such underplating below the eastern TAC is evidenced by the presence of numerous mafic dikes and sills. The underplated mafic melts may have induced a high thermal gradient and lead to relative uplift of the lower crust leading to crustal scale tilting of the Neoarchaean domain observed from east to west (Fig. 10A). This is supported by the younging of U–Pb ages and the occurrence of upper crustal granodioritic rocks to the west. Therefore, the main structure of the Neoarchaean domain of the TAC appears to be related to this 2.5–2.4 Ga tectonometamorphic event.

(2) The opening of the intracontinental Cape Hunter and Dumont D'Urville basins can be related to a Paleoproterozoic extensional phase (Fig. 10B). These basins opened synchronously and the minimum age of sediment deposition is constrained by the youngest detrital core zircons ages at 1.76 G and 1.72 G dated in the Cape Hunter phyllites and the DDU migmatites respectively (Oliver and Fanning, 1997; Peucat et al., 1999a). The protolith of the DDU gneisses (Monnier et al., 1996) indicates a sedimentary origin that might correspond to a mature rift system with strong erosion and transport and to a subordinate silica-rich igneous contribution (Peucat et al., 1999a). A comparable origin was inferred by Oliver and Fanning (1997) for the Cape Hunter metasediments. The narrow shape of the Cape Hunter Basin is suggested by its extension to the Price Island phyllites, in the South Australian Gawler craton (Oliver and Fanning, 1997). Such a geometry fits well with a transtensive depositional context. In contrast, the Dumont D'Urville basin seems to represent a wider structure with regard to its very thick sediment pile and its regional extension.

(3) Following this stage, a Paleoproterozoic transpressive phase is identified by HT metamorphism, crustal anatexis and mantle derived magmatism (Fig. 8F) within the DDU basin (Pointe Géologie area, Peucat et al., 1999a; Pelletier et al., 2002) and new $^{40}Ar/^{39}Ar$ ages obtained essentially in the intermediate to upper crustal Neoarchaean domain and within the basins (Fig. 10C).

In the Neoarchaean domain, this 1.7 Ga tectono-metamorphic event is indicated by an anastomosing shear zone network indicating a global E–W to NE–SW shortening event with slight strike-slip component and recrystallization associated with fluid circulation in decimetre to metre-scale shear zones. This tectono-metamorphic event is discrete in the Neoarchaean basement, where it only reactivates previous transcurrent structures. *Ca.* 2.5 Ga U–Pb ages are well preserved and have only been reset in highly strained zones due to intense strain overprinting in the greenschist facies conditions with high fluid/rock ratio. Partial to total resetting of the Ar/Ar amphibole chronometer (Di Vincenzo et al., 2007) implies that the peak temperature slightly exceeded 550 °C (Villa, 1998) inside the Neoarchaean domain.

Along the N30 Mertz shear zone, deformation is mainly coaxial, associated with conjugate sinistral N140 shear bands. Neoarchaean granulite tectonic lenses were observed in the field within the shear zone suggesting a positive flower structure with exhumation of large rigid blocks in the centre of the shear zone. Outside of the granulite lenses, deformation occurred at the ductile/brittle transition (350–400 °C) as evidenced by biotite/chlorite recrystallization and the cataclastic fabric of quartz and feldspar along shear zones.

In the Paleoproterozoic basins, The Cape Hunter phyllites display upright folding with a vertical foliation and sub-vertical fold axes. This is consistent with horizontal shortening during basin closure.

In the Dumont D'Urville basin, Pelletier et al. (2002), and Gapais et al. (2008) describe a deformation gradient from dome-shaped structures to the west to vertical shear zones to the east. U–Pb ages date the metamorphic peak conditions at 1.69 Ga for the entire Dumont D'Urville basin. In contrast, $^{40}Ar/^{39}Ar$ amphibole and biotite ages show a W–E gradient with increasing ages toward the basin's eastern rim. Within the basin, in the Pointe Géologie area, the exhumation rate is low at 0.1 mm yr^{-1} and increases eastward up to 0.2 mm yr^{-1}, in the Cap Jules area (Fig. 9). These contrasting exhumation rates are consistent with the deformation gradient. In fact, in a transpressive context, vertical motions are partitioned and increase at the vicinity of the main shear zone (Fossen and Tikoff, 1998; Cruden et al., 2006; Cagnard et al., 2006). In comparison to modern orogens, such tectonic uplift rates are one order of magnitude lower. For instance uplift rates of 3 mm yr^{-1} are estimated in the high Karakoram range and about 1 mm yr^{-1} in the French Alps (Rolland et al., 2001, 2007). This could be explained either by a slower convergence rate, or a different deformation mode of the warm lithosphere. In the absence of any estimate of paleo-convergence rates, we cannot discuss the former hypothesis. Nevertheless, horizontal flow and tangential movements dominate vertical motions within a warm lithosphere and are the key mechanisms that control the large-scale deformation style (Rey and Houseman, 2006; Duclaux et al., 2007; Gapais et al., 2008).

(4) A ~1550–1500 Ma event is solely recorded in the Neoarchaean basement by complete resetting of $^{40}Ar/^{39}Ar$ biotite and partial resetting of $^{40}Ar/^{39}Ar$ amphibole ages within a restricted area of 20 km wide along the Mertz Shear zone (from Correll Mount to Stillwell Island). Direct age measurements undertaken on the Mertz shear zone samples record a last geochronological event at 1509 Ma (Di Vicenzo et al., 2007), corresponding to greenschist grade biotite and chlorite recrystallization. The significance of this ~1.5 Ga event is still not clearly established. Thermal overprinting during this event is not pervasive within the entire Neoarchean and Paleoproterozoic crystalline basement. It is shown to affect mainly the Mertz high-strain zone, where mylonitic deformation and associated upper greenschist facies metamorphism have occurred. Have the Ar system been reset only where extensive fluid flow was focussed *i.e.* in the main shear zone, while a thermal event of *ca.* 300 °C occurred in the whole region? Or does this age group represent a thermal event restricted to the eastern border of the region? From our observations, it is still difficult to answer

this question. However, we can note from our studied sample (*i.e.* GD04-120) that a static recrystallization of biotite has occurred even in the shear zone core. Thus, we interpret this event as a phase of recrystallization due to intense fluid circulation that mimics some thermal overprinting. At the regional scale, this event is contemporaneous with the activation of major shear zones within the Gawler Craton in South Australia (Swain et al., 2005). In this global context, the Mertz Shear zone may act as a major plumbing system for fluid circulation at around 1550–1500 Ma. Furthermore, the Mertz shear zone is a major boundary between East and West Antarctica, and further reworking may possibly have occurred later under very low grade and probably brittle conditions.

6. Conclusions

The combination of structural and geochronological studies allows us to propose a detailed geological scenario for the TAC, from the Neoarchaean to the Mesoproterozoic.

(1) During the Archaean period: following a period of crustal generation prior to 2.6 Ga, the Neoarchaean domain underwent a major tectono-metamorphic event at *ca.* 2.44 Ga. Retrogression from granulite to amphibolite occurred within a short time period before 2.44 Ga. Exhumation of lower granulitic crust occurred within a dome-shaped structure and juxtaposition with the upper to intermediate subdomain took place during this orogenic episode (Ménot et al., 2005; Duclaux et al., 2007).
(2) During the Paleoproterozoic period: basin opening occurred in a transtensive tectonic context within and above the already exhumed Archaean basement, rapidly followed by basin closure at *ca.* 1.7 Ga. Within the already cooled Archaean domain, deformation at the ductile/brittle transition is localized in metre-scale anastomozed shear zones. The Mertz shear Zone is active during this period and featured by intense tectonic reactivation. In the DDU basin, the HT deformation is more penetrative at hectometre-scale. Despite slightly contrasted uplift rates between the rim and the centre of the basin, exhumation rates remain low (0.1–0.2 mm yr^{-1}) reflecting massive horizontal flow in the Paleoproterozoic crust.
(3) During the Mesoproterozoic period: partial resetting occurred within a narrow zone along the Mertz Shear zone which acts as passive plumbing system for fluid transfers.

Usually, in general models of continent generation, terranes amalgamation are discussed in order to explain crustal growth processes. In the TAC case, Paleoproterozoic basins seem to have opened directly on the Archaean basement and recycled this older crust. Consequently, the TAC is a good example of intracontinental evolution without any evidence of subduction, suture zone and oceanic accretionary collage. Whether general changes in the deformation style occurred at this time period on Earth, they cannot be proven by only looking at this one region as the tectonic history and deformation styles are intimately interlinked with the prevailing *P–T* conditions of the crustal regime now exposed for us to examine.

Acknowledgements

This work has been conducted with help and the logistics provided by the French Polar Institute (IPEV) in the frame of the GEOLETA program. Additional funding for analyses was provided by the CNRS (DYETI) program entitled "Deformation of anomalously hot Lithospheres". We wish to thank the support of the technical staff in Saint-Etienne, Lyon and Nice universities, who assisted with sample preparation and data acquisition. We thank G. Féraud for his help with the $^{40}Ar/^{39}Ar$ analysis. C. Clark and S. Harley are warmly thank for their helpful suggestions, which improved the quality of the manuscript. GD thanks N. Lazima for improving the English of the manuscript.

Appendix A. Analytical procedure and data processing (Gongalves et al., 2004)

The theoretical basis and associated statistical treatment of data follow the analytical procedure detailed by Montel et al. (1996). Measurements were performed on a Cameca SX100 electron microprobe at the Laboratoire Magmas et Volcans, Clermont-Ferrand, and on a Camebax electron microproble at the Laboratoire des Sciences de la Terre, Lyon.

Analytical conditions include an accelerating voltage of 15 kV and a beam current of 150 nA. U and Th were analysed successively with a PET crystal on the same wavelength-dispersive spectrometer with a counting time of 225 s and 75 s on peak, respectively. Pb was analysed with an LPET crystal using a 300 s counting time on peak. P, Ca, Si and Y were analysed successively with a PET crystal on the same spectrometer with a 30 s counting time for P and Ca, and 90 s for Si and Y. Light rare earth elements (LREE; La, Ce, Pr, Nd, Sm and Gd) were analysed using an LIF crystal with counting time of 30 s for La and Ce, 45 s for Pr and Nd, and 60 s for Sm and Gd. Counting time for the background corresponds to half of peak time for each element, on both sides of the peak. X-ray lines and background offsets, which were not always symmetrical with respect to the peak, were selected to minimize the X-ray line interferences. X-ray lines selected were: Kα for P, Ca and Si; Lα for Y, La and Ce; Lβ for Pr, Nd, Sm and Gd; Mα for Th and Pb; Mβ for U. The Pb Mα–Y Lγ overlap correction factor was 0.0018. The U Mβ–Th Mγ overlap was not corrected.

Standards used were UO_2 and ThO_2 for U and Th, apatite for Ca, zircon for Si, and synthetic phosphates for the REE, P and Y ($LaPO_4$, $CePO_4$, etc.). For Pb, a synthetic glass was used for calibration. Beam current used for standards was 100 nA. Counting time was 50 s on peak and 20 s on background for UO_2 and ThO_2, and 300 s on peak and 100 s on background for PbO. Counting times for LREE and other elements (Ca, Si, P and Y) were 80 s and 40 s respectively on peak, and 20 s and 10 s respectively on background. Errors in U, Th and Pb contents and detection limits were calculated using the procedure of Ancey et al. (1978).

Individual ages, which are referred to as measurements, were calculated from the U, Th and Pb concentrations. The 2σ errors given on measurements depend on U, Th and Pb contents and were calculated by propagating the uncertainties in these elements (at the 95% confidence level) into the decay equation. Samples ages and associated errors (with 95% confidence level) were calculated by averaging the individual measurements assuming that they belong to a single population. A least-squares modelling approach was applied to the whole population of measurements to identify multiple populations (Montel et al., 1996). The quality of the modelling is assessed from the mean square of weighted deviates (MSWD). The whole measurement population is graphically depicted in weighted histograms, where each measurement and its uncertainty are represented by bell-shaped probability curves.

A study by Jercinovic and Williams (2005) has demonstrated that inaccurate background subtraction and interference correction can lead to dramatic errors of 50 Ma or more in EMP dating when concentrations approach the trace element range. Because our background was estimated via a simple two-point linear interpola-

tion and U Mβ–Th Mγ interference was not considered, variations below 50 Ma in chemical ages have not been over-interpreted in this study.

Appendix B. Detailed presentation of the monazite dating results

In the following paragraph, we provide details of monazites age modelling by location, from East to West.

Along the MSZ at Aurora Peak, tiny monazites within shear bands of Opx-Pl-Qtz mylonites samples RPM98-119 and RPM98-124b display one statistical population age at 1619 ± 48 Ma (MSWD 0.97, $n = 10$), defining the peak of tectonic activity, and older inheritance with a bulk age at 1890 ± 52 Ma ($n = 4$).

On Close Island, large monazites from the migmatite gneiss sample GD04-174 record a single monazite population age at *ca.* 2530 Ma (A. Fernandez, pers. com.).

Further west, on the Hodgeman Archipelago, granulitic migmatite gneisses GD04-162 and GD04-160a display 2 statistical population ages from large monazites included in garnet and feldspar, at 2477 ± 22 Ma (MSWD 2.66, $n = 15$) and 2282 ± 40 Ma (MSWD 0.7, $n = 8$). The first population age is interpreted to reflect the time of the granulite facies metamorphic peak, and the latter may relate to some Th–U–Pb system partial resetting or late fluid circulation and rejuvenation of monazites by Pb loss.

Within the Watt Bay, samples from two locations have been dated. Small monazites from Al-rich metapelites GD04-155 and RPM03-34, associated with marbles and calc-silicates, represent one poorly constrain population at 1755 ± 54 Ma (MSWD 2.37, $n = 4$) and record some older inheritance at 2094 ± 180 Ma (MSWD 0.09, $n = 2$). As the first age is interpreted as reflecting dynamic recrystallization and CO_2 bearing fluid circulation during a tectono-thermal event, the second may just represent some partially resetted relicts from an earlier event.

On C Island, we selected three samples for their interesting textures and meaningful field relationships. A hydrated mylonitic shear zone (GD04-147) dated at 1696 ± 44 Ma (MSWD 0.76, $n = 6$) cross-cut an istotropic hectometric tonalitic body (GD04-149) dated at 2433 ± 34 Ma (MSWD 1.18, $n = 11$) that includes a foliated granulitic mafic xenoliths (GD04-148) dated at 2629 ± 22 Ma (MSWD 2.50, $n = 14$).

On the Cape Pigeon, two orthogneissic samples, GD04-130 and GD04-133, in the vicinity of a steep shear zone described in Ménot et al. (2005), record two statistical populations ages. The first is well defined at 1697 ± 44 Ma (MSWD 0.37, $n = 11$), and the second is defined at 1869 ± 70 Ma (MSWD 1.2, $n = 4$). The *ca.* 1700 Ma age might correspond to the reactivation and dynamic recrystallization along the shear zone, whereas the older age might correspond to partial resetting of an older age or to an earlier tectonic activity but has to be taken with care regarding the low numbers of analyses.

On Stillwell Island, an intrusive granite body including relictual garnets records two monazite population ages at 2468 ± 44 Ma (MSWD 0.7, $n = 6$) from monazites included in the qtz-pl matrix and 2586 ± 38 Ma (MSWD 0.47, $n = 9$) from monazites included in garnets.

Some tens of kilometres more to the west on the boundary of the deep subdomain, on Fletcher C Island a fluid rich mylonite (GD04-190) displays 2 population ages at 1897 ± 28 Ma (MSWD 1.59, $n = 10$) and 1712 ± 34 Ma (MSWD 2.81, $n = 6$).

References

Alexandrov, P., Ruffet, G., Cheilletz, A., 2002. Muscovite recrystallization and saddle-shaped $^{40}Ar/^{39}Ar$ age spectra: example from the Blond granite (Massif Central, France). Geochimica et Cosmochimica Acta 66 (10), 1793–1807.

Ancey, M., Bastenaire, F., Tixier, R., 1978. Application des méthodes statistiques en microanalyse. In: Maurice, F., Menyand, L., Tixier, R. (Eds.), Microanalyse, Microscopie Électronique à Balayage. Les éditions du physicien, Orsay, pp. 323–347.

Arnaud, N.O., Kelley, S.P., 1995. Evidence for excess argon during high pressure metamorphism in the Dora Maira Massif (Western Alps, Italy), using an ultra-violet laser ablation microprobe $^{40}Ar–^{39}Ar$ technique. Contributions to Mineralogy and Petrology 121, 1–11.

Cagnard, F., Durrieu, N., Gapais, D., Brun, J.P., Ehlers, C., 2006. Crustal thickening and lateral flow during compression of hot lithospheres, with particular reference to precambrian times. Terra Nova 18 (1), 72–78.

Castonguay, S., Ruffet, G., Tremblay, A., Féraud, G., 2001. Tectonometamorphic evolution of the Southern Quebec Appalachians: $^{40}Ar/^{39}Ar$ evidence for Middle Ordovician crustal thickening and Silurian-Early Devonian exhumation of the internal Humber zone. Bulletin of the Geological Society of America 113 (1), 144–160.

Chardon, D., Peucat, J.J., Jayananda, M., Choukroune, P., Fanning, C.M., 2002. Archean granite-greenstone tectonics at Kolar (South India): interplay of diapirism and bulk inho-mogeneous contraction during juvenile magmatic accretion. Tectonics 21 (3), 7-1-7-17.

Cheilletz, A., Ruffet, G., Marignac, C., Kolli, O., Gasquet, D., Feraud, G., Bouillin, J.P., 1999. $^{40}Ar/^{39}Ar$ dating of shear zones in the Variscan basement of Greater Kabylia (Algeria). Evidence of an Eo-Alpine event at 128 Ma (Hauterivian-Barremian boundary): geodynamic consequences. Tectonophysics 306 (1), 97–116.

Collins, A.S., Reddy, S.M., Buchan, C., Mruma, A., 2004. Temporal constraints on Palaeoproterozoic eclogite formation and exhumation (Usagaran Orogen, Tanzania). Earth and Planetary Science Letters 224 (1–2), 177–194.

Cruden, A.R., Nasseri, M.H.B., Pysklywec, R., 2006. Surface topography and internal strain variation in wide hot orogens from three-dimensional analogue and two-dimensional numerical vice models. Geological Society Special Publication 253, 79–104.

Di Vincenzo, G., Talarico, F., Kleinschmidt, G., 2007. An $^{40}Ar–^{39}Ar$ investigation of the Mertz Glacier area (George V Land, Antarctica): implications for the Ross Orogen–East Antarctic Craton relationship and Gondwana reconstruction. Precambrian Research 152, 93–118.

Duclaux, G., Rey, P., Guillot, S., Ménot, R.P., 2007. Orogen-parallel flow during continental convergence: numerical experiments and Archean field examples. Geology 35 (8), 715–718.

Duclaux, G., 2007. Comportement mécanique des lithosphères continentals chaudes – Evolutions des cratons Néoarchéens et Paléoprotérozoïques de Terre Adélie (Antarctique Est) et du Gawler (South Australia). Ph.D. Thesis, Université Jean Monnet & The University of Sydney. Available from: <http://tel.archives-ouvertes.fr/index.php?halsid=2gl9idaauh94pqnnh8djb9j544&view_this_doc=tel-00206311&version=1>.

Fanning, C.M., Daly, S.J., Bennett, V.C., Ménot, R.P., Peucat, J.J., Oliver, R.L., 1995. The "Mawson Block": once contiguous Archean to Proterozoic crust in the East Antarctic Shield and Gawler Craton, Australia. In: VII International Symposium on Antartic Earth Sciences, 10–15/09/1995, Sienna, Italy.

Fanning, C.M., Ménot, R.P., Peucat, J.J., Pelletier, A., 2002. A closer examination of the direct links between southern Australia and Terre Adélie and George V Land. In: Preiss, V.P. (Ed.), Geosciences 2002, Expanding Horizons. Abstracts of the 16th Australian Geological Conference, vol. 67. Adelaide, p. 224.

Fanning, C.M., Peucat, J.J., Ménot, R.P., 2003. Whither the Mawson continent? 9th ISAES, Potsdam, Abstract.

Finger, F., Krenn, E., 2007. Three metamorphic monazite generations in a high-pressure rock from the Bohemian Massif and the potentially important role of apatite in stimulating polyphase monazite growth along PT loop. Lithos 95, 103–115, doi:10.1016/j.lithos.2006.06.003.

Fitzsimons, I.C.W., 2000. A review of tectonic events in the East Antarctic shield and their implications for Gondwana and earlier Supercontinents. Journal of African Earth Sciences 31 (1), 3–23.

Fitzsimons, I.C.W., 2003. Proterozoic basement provinces of southern and south-western Australia and their correlation with Antarctica. In: Yoshida, M., Windley, B.F., Dasgupta, S. (Eds.), Proterozoic East Gondwana: Supercontinent Assembly and Breakup, vol. 206. Geological Society, Special Publications, London, pp. 93–130.

Fossen, H., Tikoff, B., 1998. Extended models of transpression and transtension, and application to tectonic settings. Geological Society Special Publication (135), 15–33.

Gapais, D., Pelletier, A., Menot, R.P., Peucat, J.J., 2008. Paleoproterozoic tectonics in the Terre Adelie Craton (East Antarctica). Precambrian Research 162 (3–4), 531–539.

Goncalves, P., Nicollet, C., Montel, J.M., 2004. Petrology and in situ U–Th–Pb monazite geochronology of ultrahigh-temperature metamorphism from the Andriamena mafic unit, north-central Madagascar. Significance of a petrographical *P–T* path in a polymetamorphic context. Journal of Petrology 45, 1923–1957.

Hamilton, W., 1998. Archean tectonics and magmatism. International Geology Review 40 (1), 1–39.

Harrison, T.M., Duncan, I., Mc Dougall, I., 1985. Diffusion of ^{40}Ar in biotite: temperature, pressure and compositional effects. Geochimica et Cosmochimica Acta 49, 2461–2468.

Jercinovic, M.J., Williams, M.L., 2005. Analytical perils (and progress) in electron microprobe trace element analysis applied to geochronology: background acquisition interferences, and beam irradiation effects. Am. Mineral. 9, 526–546.

Jourdan, F., Verati, C., Feraud, G., 2006. Intercalibration of the Hb3gr $^{40}Ar/^{39}Ar$ dating standard. Chemical Geology 231 (3), 177–189.

Leloup, P.H., Arnaud, N., Sobel, E.R., Lacassin, R., 2005. Alpine thermal and structural evolution of the highest external crystalline massif: The Mont Blanc. Tectonics 24, TC4002, doi:10.1029/2004TC001676.

Ménot, R.P., Peucat, J.J., Pelletier, A., Fanning, M., 1999. New constrains on the Archean - Proterozoic evolution of the Terre Adélie - George V Land, East Antartica. EUG 10, Strasbourg, March 28–Apri1 1999. Abstract vol. 122.

Ménot, R.P., Pêcher, A., Rolland, Y., Peucat, J.J., Pelletier, A., Duclaux, G., Guillot, S., 2005. Structural setting of the Neoarchean terrains in the Commonwealth Bay Area (143–145°E), Terre Adélie Craton, East Antarctica. Gondwana Research 8, 1–9.

Ménot, R.P., Duclaux, G., Peucat, J.J., Rolland, Y., Guillot, S., Fanning, M., Bascou, J., Gapais, D., Pêcher, A., 2007. Geology of the Terre Adélie Craton (135–146°E). In: Cooper, A.K., Raymond, C.R., et al. (Eds.) Antarctica: a Keystone in a Changing World – Online Proceedings of the 10th ISAES, USGS Open-File Report 2007-1047, Short Research Paper 048, 5 pp., doi:10.3133/of2007-1047.srp048.

Monnier, O., 1995. Le socle protérozoique de Terre Adélie (Antarctique Est): son évolution tectono-métamorphique et sa place dans dans les reconstitutions du Proto-Gondwana. Unpublished PhD thesis, Université de Saint Etienne, 321 pp.

Monnier, O., Ménot, R.P., Peucat, J.J., Fanning, M., Giret, A., 1996. Actualisation des données géologiques sur Terre Adélie (Antarctique Est): mise en évidence d'un collage tectonique au Paléoprotérozoïque, Comptes Rendus De L Academie Des Sciences, Paris 322, IIa, 55–62.

Montel, J.M., Foret, S., Veschambre, M., Nicollet, C., Provost, A., 1996. Electron microprobe dating of monazite. Chemical Geology 131, 37–53.

Oliver, R.L., Fanning, C.M., 1997. Australia and Antarctica: Precise correlations of Palaeoproterozoic terrains. In: Ricci, C.A. (Ed.), The Antarctic Region: Geological Evolution and Processes. Terra Antartica Publication, Sienna, pp. 163–172.

Oliver, R.L., Fanning, C.M., 2002. Proterozoic geology east and southeast of Commonwealth Bay, George V land, Antarctica, and its relationship to that of adjacent Gondwana terranes. In: Gamble, J.A., Skinner, D.N.B., Henry, S. (Eds.), Antarctic at the Close of a Millennium, The Royal Society of New Zealand Bulletin 35, 51–58.

Pelletier, A., Gapais, D., Ménot, R.P., Guiraud, M., 1999. The 1.7 Ga tectonic and metamorphic event in the Terre Adélie Craton (East Antarctica). In: 8th International Symposium on Antarctic Earth Sciences, Wellington, NZ, July, Abstract vol. 239.

Pelletier, A., Ménot, R.P., Gapais, D., Peucat J.J., 2001. Late Archaen to Paleoproterozoic Structural and Metamorphic Evolution in the Terre Adélie Craton – East Antarctica, poster presentation, EUG 2001, Strasbourg, abstract p. 71.

Pelletier, A., Gapais, D., Ménot, R.P., Peucat, J.J., 2002. Tectonique transpressive en Terre Adélie au Paléoprotérozoïque (Est Antarctique). Comptes Rendus Geoscience 334, 505–511.

Peucat, J.J., Ménot, R.P., Monnier, O., Fanning, C.M., 1999a. The Terre Adélie basement in the East Antarctica Shield: geological and isotopic evidence for a major 1.7 Ga thermal event; comparison with the Gawler Craton in South Australia. Precambrian Research 94, 205–224.

Peucat, J.J., Ménot, R.P., Fanning, C.M., Pelletier, A., Pecora, L., 1999b. Geochronological evidence for a Late-Archean basement in the Terre Adélie Craton, 8th ISAES, Wellington, NZ, p. 242.

Rey, P.F., Houseman, G., 2006. Lithospheric scale gravitational flow: the impact of body forces on orogenic processes from Archaean to Phanerozoic. Geological Society Special Publication 253, 153–167.

Roddick, J.C., 1983. High precision intercalibration of ^{40}Ar–^{39}Ar standards. Geochimica et Cosmochimica Acta 47 (5), 887–898.

Rolland, Y., Mahéo, G., Guillot, S., Pêcher, A., 2001. Tectono-metamorphic evolution of the Karakoram Metamorphic Complex (Dassu-Askole area, NE Pakistan): exhumation of mid-crustal HT-MP gneisses in a convergent context. Journal of Metamorphic Geology 19, 717–737.

Rolland, Y., Corsini, M., Rossi, M. Cox, S.F., Pennacchioni, G., Mancktelow, N., Boullier, A.M., 2007. Comment on the dating of Alpine deformation by Ar–Ar on syn-kinematic mica in mid-crustal shear zones of the Mont Blanc Massif (paper by Leloup et al.). Tectonics 26, TC2015, doi:10.1029/2006TC001956.

Rolland, Y., Rossi, M., Cox, S.F., Corsini, M., Mancktelow, N., Pennacchioni, G., Fornari, M., Boullier, A.M., 2008. ^{40}Ar/^{39}Ar dating of syn-kinematic white mica: insights from fluid-rock reaction in low-grade shear zones (Mont Blanc Massif) and constraints on timing of deformation in the NW External Alps. In: Wibberley, C.A.J., Kurtz, W., Imber J., Holdsworth, R.E., Colletini, C. (Eds.), The Internal Structure of Fault Zones: Implications for Mechanical and Fluid-Flow Properties. Geological Society of London Special Publications 299, 293–315, doi:10.1144/SP299.17.

Ruffet, G., Feraud, G., Amouric, M., 1991. Comparison of ^{40}Ar–^{39}Ar conventional and laser dating of biotites from the North Tregor Batholith. Geochimica et Cosmochimica Acta 55 (6), 1675–1688.

Ruffet, G., Feraud, G., Balevre, M., Kienast, J.R., 1995. Plateau ages and excess argon in phengites: an ^{40}Ar–^{39}Ar laser probe study of Alpine micas (Sesia Zone, Western Alps, northern Italy). Chemical Geology 121 (1–4), 327–343.

Suzuki, K., Adachi, M., Tanaka, T., 1991. Middle Precambrian provenance of Jurassic sandstone in the Mino Terrane, central Japan: Th–U–total Pb evidence from an electron microprobe monazite study. Sedimentary Geology 75 (1–2), 141–147.

Swain, G.M., Hand, M., Teasdale, J., Rutherford, L., Clark, C., 2005. Age constraints on terrane-scale shear zones in the Gawler Craton, southern Australia. Precambrian Research 139 (3–4), 164–180.

Talarico, F., Kleinschmidt, G., 2003. Structural and metamorphic evolution of the Mertz Shear Zone (East Antarctica Craton, George V Land): implications for Australia/Antarctica correlations and East Antarctic Craton/Ross Orogen relationships. Terra Antartica 10, 229–248.

Tapponnier, P., Peltzer, G., Le Dain, A.Y., Armijo, R., Cobbold, P., 1982. Propagating extrusion tectonics in Asia: new insights from simple experiments with plasticine. Geology 10, 611–616.

Tingey, R.J., 1991. The regional geology of Archaean and Proterozoic rocks in Antarctica. In: Tingey, R.J. (Ed.), The Geology of Antarctica. Oxford University Press, Oxford, pp. 1–73.

Turner, G., Huneke, J.C., Podosek, F.A., Wasserburg, G.J., 1971. ^{40}Ar–^{39}Ar ages and cosmic ray exposure ages of Apollo 14 samples. Earth and Planetary Science Letters 12 (1), 19–35.

Villa, I.M., 1998. Isotopic closure. Terra Nova 10 (1), 42–47.

Wendt, I., Carl, C., 1991. The statistical distribution of the mean squared weighted deviation. Chemical Geology (Isotope Geoscience Section) 86 (4), 275–285.

Wing, B.A., Ferry, J.M., Harrison, T.M., 2003. Prograde destruction and formation of monazite and allanite during contact and regional metamorphism of pelites: petrology and geochronology. Contributions to Mineralogy and Petrology 145 (2), 228–250.